# Beamforming Design in Reconfigurable Intelligent Surface-Assisted IoT Networks Based on Discrete Phase Shifters and Imperfect CSI

Sajjad Nassirpour, Alireza Vahid, Dinh-Thuan Do, and Dinesh Bharadia

***Abstract*—In this paper, we study reconfigurable intelligent surface (RIS)-assisted networks to support Internet of Things (IoT) devices. We propose RIS beamforming strategies to maximize sum-rate and fairness and analyze the RIS location. We derive a theoretical lower-bound of the minimum number of RIS elements needed to guarantee specific network performance metrics and validate our results via simulations. We present two RIS scenarios in this study, both with the same total number of RIS elements: (i) centralized RIS, where a single RIS assists the network, and (ii) distributed RIS, where each transmitter has its own dedicated RIS. We study addressing two practical challenges related to RIS elements and channel state information (CSI) assumptions. First, we consider hardware limitations by assuming that each RIS element is equipped with a discrete phase shifter (PS). Second, we investigate the impact of CSI perfectness and availability in the network; therefore, we evaluate the performance of the RIS-assisted network under two scenarios: (a) centralized RIS with imperfect global CSI and (b) distributed RIS, where imperfect local CSI is available at each transmitter.**

***Index Terms*—Beamforming, Internet of Things, distributed transmitters, reconfigurable intelligent surface, integer programming, fading channels, throughput, channel state information.**

## I. Introduction

In the past few years, Internet of Things (IoT) communication networks have enabled devices with sensing, processing, and communication capabilities to provide a wide range of services, such as intelligent manufacturing, emergency detection, and structural health monitoring with minimal human interaction [1]. To fully utilize the potential of IoT networks, two research challenges need to be addressed. Firstly, the issue of massive connectivity is foreseen as hundreds of billions of IoT devices will be in operation by 2030 [2], and this results in a co-channel interference issue. Secondly, many IoT devices rely on batteries, which are supposed to last for ten years or more, and this necessitates to development of power-efficient solutions [3]. To address these challenges, one solution is to allocate a unique chunk of spectrum to each IoT device, which is not a scalable solution due to the scarcity of the spectrum. Furthermore, massive multiple-input multiple-output (MIMO) with a large number of antennas is an attractive beamforming technique to support IoT devices, which creates a focused beam for the desired IoT device while simultaneously providing nulls at undesired devices. Nevertheless, this approach is power-hungry as each antenna is connected to a single radio frequency (RF) chain, thereby increasing the complexity and cost of the method.

A promising application of programmable metasurfaces called reconfigurable-intelligent-surface (RIS) has been recently introduced. An RIS comprises a large number of passive elements, specifically phase shifters (PSs), that are intelligently tuned to substantially improve wireless communication performance. On the one hand, RIS has the capability to enhance signal quality, making it possible to accommodate IoT devices in scenarios with massive connectivity. Moreover, RIS offers low-cost hardware with low-power consumption due to its passive reflectors. As a result, RIS could be a solution to respond to the aforementioned challenges and therefore has found a vast number of applications in IoT networks, including but not limited to joint beamforming to enhance over-the-air computation [4], improving secrecy rate [5], and unmanned aerial vehicle (UAV) communications [6].

### A. State-of-the-art

The exceptional features of RIS have garnered significant attention from both academia and industry, leading to apply RIS-based beamforming techniques to enhance the performance of wireless communication networks, such as maximizing the sum-rate and improving fairness among the IoT devices [7–9]. In particular, [7] studied an RIS-assisted multi-user multiple-input single-output (MISO) wireless-powered communication network, where the users harvest energy in the downlink and transmit their information simultaneously in the uplink to a single access point (AP). In [7], the authors maximized the weighted sum-rate by jointly optimizing the active beamforming at the AP and the passive beamforming at RIS. Next, the authors in [9] investigated an RIS-assisted multi-cell MISO network to suppress the inter-cell interference. They focused on a max-min fairness problem and applied an alternative optimization (AO) method to jointly optimize the AP beamforming and the RIS elements.

As we mentioned earlier, IoT networks confront a massive connectivity challenge. Consequently, assuming distributed

S. Nassirpour is with the Department of Electrical Engineering at the University of Colorado Denver, Denver, CO 80204, USA. Email: sajjad.nassirpour@ucdenver.edu.

A. Vahid is with the Department of Electrical and Microelectronic Engineering at Rochester Institute of Technology, Rochester, NY 14623, USA. Email: arveme@rit.edu.

D.-T. Do is with the School of Engineering, University of Mount Union, Alliance, OH 44601, USA. Email: doth@mountunion.edu.

D. Bharadia is with the Department of Electrical and Computer Engineering at the University of California, San Diego, CA 92093, USA. Email: dineshb@eng.ucsd.edu.

APs in the network supporting multiple IoT devices is a more realistic scenario. Motivated by this, [10] considered an RIS-assisted MIMO device-to-device network with distributed APs and then maximized the achievable degrees of freedom (DoF) by jointly designing the PSs at RIS and transceiver coding matrices. However, the extent to which RIS beamforming and active beamforming at the transceivers contribute to the overall benefit is unclear. Therefore, in the first part of this work, similar to [11], we focus on pure RIS gain by considering a single-input single-output (SISO) network with distributed APs that uses a single RIS, which we refer to as a centralized RIS, to support multiple IoT devices. Here, we design RIS beamforming to maximize sum-rate and optimize fairness.

Previous studies have typically considered Rayleigh fading for channels without a line of sight (LoS), Rician fading for channels with an LoS link, and Nakagami fading for scenarios involving multi-path where one path is non-LoS but stronger [7–10, 12]. In our work, we comprehensively evaluate the performance of our RIS-assisted network under Rayleigh, Rician, and Nakagami fading models.

The construction of a PS with infinite-bit resolution is difficult due to manufacturing issues [13]. Thus, discrete PSs are utilized in real-world scenarios, which turn the optimization problem into a non-convex nonlinear integer programming (NLIP) problem that is NP-hard. To the best of our knowledge, a brute-force search is the only method to obtain the global optimum solution of an NLIP problem, which examines all possible solutions. However, the brute-force search is not a practical approach due to its extremely high complexity. Thus, in [14, 15], the authors proposed a successive-refinement (SR) algorithm to optimize the discrete PSs at RIS. However, this approach only provides local optimal solutions. In this paper, we introduce a low-complexity optimization method based on filled function, which directly targets discrete PSs to optimize the RIS elements and uses filled function to move from one local optimum solution to a better one.

Apart from optimizing the RIS elements, it is important to determine the RIS location. Placing the RIS close to either the transmitter or receiver is a possible solution to mitigate the impact of product-path loss in the Tx-RIS-Rx link, but it may not always be practical due to user mobility or physical constraints. To address this issue, networks utilizing multiple RISs, referred to as the distributed RIS scenario, have been proposed to improve the performance of the RIS-assisted networks [16–20]. Specifically, a strategy based on double-RISs was proposed in [16], where one RIS is located near the AP, and the other is placed near a cluster of users. However, assuming one RIS near the users can be challenging. Next, [17] studied the statistical characterization and modeling of a network with distributed RISs, while the results were limited to a point-to-point scenario, and RIS elements were not optimized. Then, [18] focused on a distributed RIS-MIMO-non orthogonal multiple access (NOMA) system and used discrete PSs as the RIS elements, [19] proposed a distributed RIS scenario in a cell-free massive MIMO setup to maximize the sum rate, and [20] applied a beamforming technique in a MIMO network assisted by distributed RIS to optimize fairness among the users.

As RIS uses passive elements, it requires many elements to enhance the network performance, and this increases the number of channels significantly. In [18–20], the authors assumed that AP obtains perfect global channel state information (CSI) prior to communications through the pilot signals. However, in real-world scenarios, the channel estimation process faces two main challenges: (1) imperfect CSI: it is feasible to have an error in the estimation process due to hardware impairments, noise, and so on, which results in imperfect CSI, and hence affects the beamforming strategies at AP and RIS [21]; (2) CSI availability: a large number of channels in the RIS-assisted network, especially with multiple RISs, necessitates a large bandwidth for the feedback signals from the IoT devices to the AP, and this could be a bottleneck in the network. As a result, in the second part of this paper, we investigate a network with distributed RISs, where one RIS is dedicated to each AP. In this case, we assume each AP knows its outgoing imperfect channels to all IoT devices, and beyond that, it only knows the statistics of the other channels. We define this as local channel state information at transmitter (CSIT).

Moreover, we analytically derive a lower-bound of the minimum number of RIS elements needed to achieve a desired performance metric (e.g., per-user rate) and analyze the results as a function of the location of the RIS.

Table. I represents the main differences between our work and the literature.

### B. Our main contributions

We provide more details about our contributions below:

- We consider SISO RIS-assisted IoT networks with distributed transmitters. We study RIS beamforming to maximize the sum-rate and address the max-min optimization problems. We evaluate the performance of our network using relevant channel models. In particular, we first analyze the results under Rayleigh fading analytically and numerically. Then, we focus on numerical evaluation for Rician and Nakagami fading models;
- We focus on discrete PSs, which result in non-convex NLIP optimization problems. We propose a heuristic method based on the filled function to solve the problem. We compare the efficiency of our approach with two SR-based methods as well as a genetic algorithm (GA) and a simplified exhaustive search (SES) method in terms of complexity and rate;
- We study the RIS placement in our work, and quantify the minimum number of RIS elements required to achieve specific network objectives, such as sum-rate or fairness, and we validate the results through simulations, which would provide valuable practical guidelines;
- We delve into the practical considerations related to CSI perfectness and availability in RIS-assisted networks. Specifically, we examine two RIS scenarios: (1) centralized RIS, where a single RIS assists the network to serve multiple IoT devices simultaneously, and imperfect CSI is available globally, and (2) distributed RIS, where each AP has its own dedicated RIS, and each AP knows its local CSIT. Notice that both scenarios utilize the same

TABLE I
MAIN DIFFERENCES BETWEEN OUR WORK AND THE LITERATURE.

| | **Our paper** | [7] | [9] | [12] | [10] | [11] | [16] | [14] | [15] | [21] | [18] | [19] | [20] |
|---|---|---|---|---|---|---|---|---|---|---|---|---|---|
| Multiple RISs | ✓ | | | | | | ✓ | | | | ✓ | ✓ | ✓ |
| Sum-rate maximization | ✓ | ✓ | | | ✓ | | | | ✓ | | | ✓ | |
| Max-min rate optimization | ✓ | | ✓ | | | | ✓ | ✓ | | | | | ✓ |
| Rayleigh fading | ✓ | ✓ | | | | | | | | ✓ | | | ✓ |
| Rician fading | ✓ | | ✓ | | ✓ | | ✓ | ✓ | ✓ | | | | |
| Nakagami fading | ✓ | | | ✓ | | | | | | | ✓ | ✓ | |
| Distributed transmitters | ✓ | | | | ✓ | ✓ | | | | | | ✓ | |
| Pure RIS gain | ✓ | | | | | ✓ | | | | | | ✓ | |
| Low-bit phase shifters | ✓ | | | | | | | ✓ | ✓ | | ✓ | | |
| Imperfect CSI | ✓ | | | | | | | | | ✓ | | | |
| Local CSIT | ✓ | | | | | | | | | | | | |
| Lower-bound on the number of RIS elements | ✓ | | | | | | | | | | | | |

total number of RIS elements to serve IoT devices. Our simulation findings indicate that the latter scenario not only achieves a higher sum-rate than the former but also requires fewer RIS elements to attain a given sum-rate.

The rest of the paper is organized as follows. We present our channel model and outline the optimization problem in Section II. In Section III, we discuss our proposed optimization approach. Then, in Section IV, we provide a lower-bound on the minimum number of required RIS elements. Section V presents the simulation results, and Section VI concludes the paper.

### C. Notations

Throughout the paper, we use bold-face lowercase, bold-face uppercase, and italic letters to denote vectors, matrices, and scalars, respectively. We also use $\mathbb{C}^{I\times J}$ to describe the space of $I\times J$ complex-valued matrices. $\mathrm{diag}\{\mathbf{x}\}$ is a diagonal matrix using vector $\mathbf{x}$, and $|\mathbf{x}|$ and $||\mathbf{x}||$ are the absolute value and Euclidean norm of complex-valued vector $\mathbf{x}$, respectively. We use $\mathbb{E}(.)$, $\log(.)$, $Re(.)$, and $Im(.)$ to denote the statistical expectation, logarithmic function in base 2, and real and imaginary parts of a complex number, respectively. Finally, $\mathbf{B}^H$ shows the conjugate transpose of matrix $\mathbf{B}$.

## II. PROBLEM SETTING

This paper focuses on an RIS-assisted IoT network with $K$ single-antenna distributed APs (transmitters) and $K$ single-antenna IoT devices (receivers). We consider two RIS-based scenarios: (1) centralized RIS, suitable when the RIS can be positioned near the transmitters or receivers, and (2) distributed RIS, where each transmitter is equipped with a dedicated RIS. Fig. 1 shows the network model, which could capture the communication dynamics of real-world IoT networks with massive connectivity, such as smart cities and Industrial IoT (IIoT) networks, where RIS(s) can be installed on building facades or factory walls, respectively.

### A. Centralized RIS

In this case, we use a centralized RIS with $M$ reconfigurable elements as shown in Fig. 1(a), where $\mathsf{Tx}_i$, RIS, and $\mathsf{Rx}_i$ are available at $(x_t^{[i]}, y_t^{[i]})$, $(x_0, y_0)$, and $(x_r^{[i]}, y_r^{[i]}), i = 1, 2, \ldots, K$, respectively.

**Channel model:** We use $h_d^{[ji]}(t) \in \mathbb{C}^{1\times 1}$, $\mathbf{h}^{[j]}(t) \in \mathbb{C}^{M\times 1}$, and $\mathbf{g}^{[i]}(t) \in \mathbb{C}^{1\times M}$ to denote the channels of $\mathsf{Tx}_j$-$\mathsf{Rx}_i$ link (between $\mathsf{Tx}_j$ and $\mathsf{Rx}_i, i, j \in \{1, 2, \ldots, K\}$), $\mathsf{Tx}_j$-RIS link, and RIS-$\mathsf{Rx}_i$ link, respectively, at time $t$. We assume RIS elements are spaced at least $\lambda/2$ apart from each other where $\lambda$ is the wavelength of the transmitted signal. Thus, the elements of $\mathbf{h}^{[j]}(t)$ and $\mathbf{g}^{[i]}(t)$ are independent across time and users.

**CSI perfectness:** We assume each receiver estimates its incoming channels from all transmitters perfectly and then informs the others about these channels through two cases: (1) The noiseless links, which represent that other network nodes learn the channels perfectly as the receiver (noiseless CSI); (2) The noisy links, meaning that the information provided to the transmitters is noisy and thus imperfect. We refer to this as "noisy-$p$" channels if other nodes attain the imperfect channels at a signal-to-noise ratio (SNR) of $p$ dB.

**CSI availability** Similar to [7–11], we assume global CSI is accessible throughout the network, and there is no further data exchange between the transmitters. Additionally, no data is exchanged beyond CSI between the receivers.

**Small-scale fading:** Similar to [22–24], since in practice, RIS is usually positioned with the knowledge of the AP's location, we consider $\mathbf{h}^{[j]}(t)$ is an LoS channel vector (i.e., $\mathbf{h}^{[j]}(t) = \mathbf{h}^{[j]}$). On the contrary, due to the user's mobility and the complex propagation environment, assuming $h_d^{[ji]}(t)$ and $\mathbf{g}^{[i]}(t)$ are LoS channels is impossible in practice; thus, we assume $h_d^{[ji]}(t)$ and $\mathbf{g}^{[i]}(t)$ are distributed based on Rayleigh fading. Here, we write $h_m^{[j]}$, the $m^{\text{th}}$ element of $\mathbf{h}^{[j]}$, as follows:

$$h_m^{[j]} = e^{-j\frac{2\pi}{\lambda}d_{\mathsf{Tx}_j-\mathrm{RIS}[m]}}, \tag{1}$$

where $d_{\mathsf{Tx}_j-\mathrm{RIS}[m]}$ shows the distance between $\mathsf{Tx}_j$ and the $m^{\text{th}}$ element of the RIS. In addition, $h_d^{[ji]}(t)$ and $g_m^{[i]}(t)$ (the $m^{\text{th}}$ element of $\mathbf{g}^{[i]}(t)$) are distributed based on $\mathcal{CN}(0, \sigma_{h_d}^2)$ and $\mathcal{CN}(0, \sigma_g^2)$, respectively, where $\sigma_{h_d}^2$ and $\sigma_g^2$ show the corresponding variances.

Later, in Section V, we will evaluate the performance of our RIS-assisted network by considering Rician and Nakagami fading models as more realistic channel fading models.

**Large-scale fading:** We use $C_0 d^{-\alpha}$ as the path loss profile where $C_0$ describes the signal loss at a reference distance (e.g., $1m$), $d$ is the distance between a pair of nodes (e.g., $\mathsf{Tx}_j$ and $\mathsf{Rx}_i$) and $\alpha$ represents the corresponding path loss exponent.

This article has been accepted for publication in IEEE Internet of Things Journal. This is the author's version which has not been fully edited and content may change prior to final publication. Citation information: DOI 10.1109/JIOT.2023.3305914



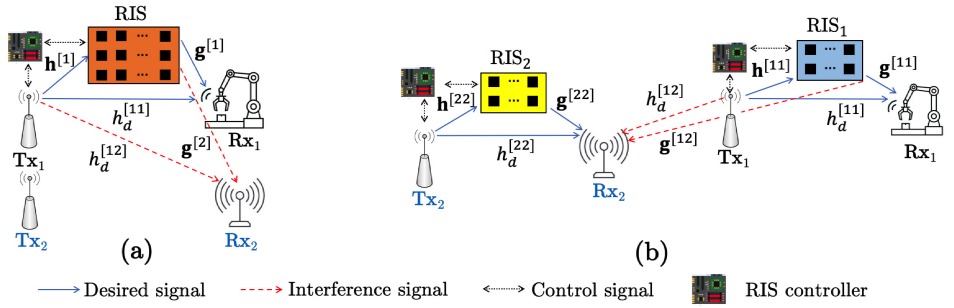


Fig. 1. *SISO IoT networks with distributed transmitters and (a) a centralized RIS, and (b) distributed RISs.*

For simplicity, in the rest of the paper, we use $m_h$, $\sigma_{h_d}^2$, and $\sigma_g^2$ to denote $h_m^{[j]}$, the variance of $h_d^{[ji]}(t)$, and the variance of each element of $\mathbf{g}^{[i]}(t)$, respectively, which include the impact of both small-scale fading and large-scale fading. In this work, we assume that the array aperture of RIS is relatively small, leading to a correspondingly small Rayleigh distance. As a consequence, the channels primarily fall within the far-field region, and the influence of the near-field is deemed negligible.

**RIS configuration:** We assume a controller between $\mathsf{Tx}_1$ and RIS to exchange CSI and control the RIS elements over a separate link. Moreover, we consider only the first reflected signal from the RIS due to the significant path loss; thus, if $\tilde{x}(t)$ is the incident signal at time $t$, we find the reflected signal from the $m^{\text{th}}$ element of the RIS as:

$$\tilde{y}_m(t) = \tilde{x}(t)\left(\beta_m(t)\, e^{j\theta_m(t)}\right), \quad 1 \le m \le M, \tag{2}$$

where $\beta_m(t) \in [0,1]$ and $\theta_m(t) \in [0, 2\pi)$ are the amplitude and phase of the $m^{\text{th}}$ element of the RIS, respectively, at time $t$. For simplicity, we consider $\beta_m(t) = 1$ in this work. We also assume that each RIS element has a $b$-bit PS, indicating that each RIS element can only take $N = 2^b$ quantized levels. We define $\phi_N$, the set of quantized values of $\theta_m(t)$, as:

$$\phi_N = \left\{0, \frac{2\pi}{N}, \frac{4\pi}{N}, \ldots, \frac{2\pi(N-1)}{N}\right\}. \tag{3}$$

Moreover, we use $\mathbf{\Theta}(t) \in \mathbb{C}^{M\times M}$ to denote the RIS configuration, which is given by:

$$\mathbf{\Theta}(t) = \mathrm{diag}\{e^{\boldsymbol{\theta}(t)}\}, \quad \boldsymbol{\theta}(t) = [\theta_1(t), \theta_2(t), \ldots, \theta_M(t)]. \tag{4}$$

**Received signal:** The received signal at $\mathsf{Rx}_i$ is a combination of the direct signals from the APs and the reflected signals from the RIS, which is given by:

$$y_i(t) = \sum_{j=1}^{K}\left[\mathbf{g}^{[i]}(t)\mathbf{\Theta}(t)\mathbf{h}^{[j]} + h_d^{[ji]}(t)\right]x_j(t) + n_i(t), \tag{5}$$

where $x_j(t)$ is the transmitted signal at $\mathsf{Tx}_j$, $n_i(t) \sim \mathcal{CN}(0,\sigma^2)$ is additive white Gaussian noise (AWGN) at $\mathsf{Rx}_i$, and $\mathbb{E}\{\mathbf{x}(t)\mathbf{x}^H(t)\} = \mathrm{diag}([P_1, P_2, \ldots, P_K])$ where $\mathbf{x}(t) = [x_1(t), x_2(t), \ldots, x_K(t)] \in \mathbb{C}^{1\times K}$ and $P_j, j \in \{1, 2, \ldots K\}$ describes the transmit power from $\mathsf{Tx}_j$. As we describe later, all operations occur in a single coherence time; therefore, the time notation is removed throughout the rest of this work. In this work, we assume that the coherence time, and thus the coherence distance, is large enough so that all evaluations involve communication channels experiencing flat fading during each time slot. Then, we use (5) and write the signal-to-interference-plus-noise ratio (SINR) at $\mathsf{Rx}_i$ as follows:

$$\mathrm{SINR}_i = \frac{P_i\left|\mathbf{g}^{[i]}\mathbf{\Theta}\mathbf{h}^{[i]} + h_d^{[ii]}\right|^2}{\sigma^2 + \sum_{j=1, j\neq i}^{K} P_j\left|\mathbf{g}^{[i]}\mathbf{\Theta}\mathbf{h}^{[j]} + h_d^{[ji]}\right|^2}. \tag{6}$$

### *B. Distributed RIS*

As depicted in Fig. 1(b), we have $K$ distributed RISs, one dedicated RIS to each transmitter, where each RIS has $\frac{M}{K}$[1] elements (i.e., total RIS elements is equal to $M$). We assume the same location notations for the transmitters and the receivers as discussed in Section II-A and use $(x_0^{[i]}, y_0^{[i]})$ to denote the location of $\mathrm{RIS}_i$, the $i^{\text{th}}$ RIS.

**Channel model:** We use $\mathbf{h}^{[ji]} \in \mathbb{C}^{M\times 1}$, and $\mathbf{g}^{[ii]} \in \mathbb{C}^{1\times M}$ to denote the channels of $\mathsf{Tx}_j$-$\mathrm{RIS}_i$, $i, j = 1, 2, \ldots, K$ and $\mathrm{RIS}_i$-$\mathsf{Rx}_i$ links, respectively. Notice that $h_d^{[ji]}$, large-scale fading, and small-scale fading are similar to the case with a centralized RIS. However, since $\mathrm{RIS}_i$ is dedicated to $\mathsf{Tx}_i$, assuming LoS channels between $\mathsf{Tx}_j$ and $\mathrm{RIS}_i$ is not feasible. As a result, we assume that $\mathbf{h}^{[ji]}$ is distributed based on Rayleigh fading whose elements have $\mathcal{CN}(0, \tilde{\sigma}_h^2)$ distribution.

**CSI perfectness:** Here, we assume two channel knowledge cases as noiseless and noisy-$p$ channels.

**CSI availability:** Acquiring global CSI requires an excessive overhead because of the substantial number of channels in the RIS-assisted network. This overhead would create a bottleneck in practice as feedback channels have limited bandwidth [25–30] and the delay overhead may render forward communications infeasible [31, 32]. Therefore, in distributed RIS case, we consider no data exchange between the transmitters and focus on a more realistic assumption as $\mathsf{Tx}_i$ is aware of its outgoing channels to the receivers (the direct channels and the channels through $\mathrm{RIS}_i$) and beyond that, it only knows the statistics of the other channels. We refer to this model as local CSIT [25, 27, 28]. Further, $\mathsf{Rx}_i$ knows its incoming channels from all transmitters plus the outgoing channels from $\mathsf{Tx}_i$ to compute the optimal configuration at $\mathrm{RIS}_i$ and beyond that, it only knows the statistics of the other channels. There is no data exchange beyond CSI between the receivers.

**RIS configuration:** We assume $\mathsf{Tx}_i$ uses a controller to exchange CSI and control the PSs at $\mathrm{RIS}_i$ via a separate link. Similar to the centralized case, we consider only the first

[1]Without loss of generality, we assume $M$ is divisible by $K$.

reflected signal from each RIS and use $\theta_m^{[i]} \in \phi_N$ to denote the phase shift at the $m^{\text{th}}$ element of RIS$_i$. Then, we use $\mathbf{\Theta}^{[i]} \in \mathbb{C}^{M\times M}$ to show the RIS configuration at RIS$_i$ as:

$$\mathbf{\Theta}^{[i]} = \text{diag}\{e^{\boldsymbol{\theta}^{[i]}}\}, \quad \boldsymbol{\theta}^{[i]} = [\theta_1^{[i]}, \theta_2^{[i]}, \ldots, \theta_M^{[i]}]. \tag{7}$$

**Received signal:** According to the channel coefficients and $\mathbf{\Theta}^{[i]}$, we find the received signal at Rx$_i$, which is given by:

$$\begin{aligned} y_i = &\Big[\sum_{i'=1}^{K} \mathbf{g}^{[i'i]}\mathbf{\Theta}^{[i']}\mathbf{h}^{[ii']} + h_d^{[ii]}\Big]x_i \\ &+ \sum_{j=1,j\neq i}^{K}\Big[\sum_{i'=1}^{K} \mathbf{g}^{[i'i]}\mathbf{\Theta}^{[i']}\mathbf{h}^{[ji']} + h_d^{[ji]}\Big]x_j + n_i. \end{aligned} \tag{8}$$

Notice that the assumptions about $x_i$, transmit power $P_i$, and $n_i$ are similar to the assumptions described in (5). Based on (8), we compute the SINR at the $i^{\text{th}}$ receiver as follows:

$$\text{SINR}_i = \frac{P_i\left|\sum_{i'=1}^{K} \mathbf{g}^{[i'i]}\mathbf{\Theta}^{[i']}\mathbf{h}^{[ii']} + h_d^{[ii]}\right|^2}{\sigma^2 + \sum_{j=1,j\neq i}^{K} P_j\left|\sum_{i'=1}^{K} \mathbf{g}^{[i'i]}\mathbf{\Theta}^{[i']}\mathbf{h}^{[ji']} + h_d^{[ji]}\right|^2}. \tag{9}$$

### C. Optimization Problem

One of our goals in this work is to find the RIS configuration that maximizes the sum-rate. Therefore, we define the following optimization problem with a centralized RIS.

$$\begin{aligned} &\max_{\boldsymbol{\theta}} \underbrace{\sum_{i=1}^{K}\log(1+\text{SINR}_i)}_{\triangleq\ -q(\boldsymbol{\theta})} \equiv \min_{\boldsymbol{\theta}}\ q(\boldsymbol{\theta}) \\ &\text{s.t.}\ \ \boldsymbol{\theta} = [\theta_1, \theta_2, \ldots, \theta_M],\ \theta_m \in \phi_N,\ 1 \le m \le M. \end{aligned} \tag{10}$$

Moreover, to meet fairness among users, we define a max-min optimization problem as:

$$\begin{aligned} &\max_{\boldsymbol{\theta}} \min_{i=\{1,2,\ldots,K\}} \log(1+\text{SINR}_i) \\ &\text{s.t.}\ \ \boldsymbol{\theta} = [\theta_1, \theta_2, \ldots, \theta_M],\ \theta_m \in \phi_N,\ 1 \le m \le M. \end{aligned} \tag{11}$$

Notice that (10) and (11) are NLIP problems, and as we discussed in Section I, there is no efficient way to find the global optimum solution for them. Hence, an NLIP problem can be solved through two methods: (i) converting it to an equivalent convex approximation problem and then applying a regular convex optimizer, such as CVX [33], to find the approximated solution. In [8], the authors converted (10) into a format known as the difference of convex (DC) problem and then applied the successive convex approximation (SCA) method, an iterative approach, to find an equivalent convex form of the DC problem. Additionally, [16] focused on (11) and employed semidefinite relaxation (SDR) and bisection methods to discover a quasi-convex equivalent for (11). Nevertheless, [8, 16] made certain approximations in their approach, potentially compromising the optimality of their solutions; (ii) using a heuristic method (e.g., SR, filled function, and GA), which directly focuses on the original problem. This allows for solving both (10) and (11) using a single optimizer. In [14, 15], the authors utilized the SR-based methods, which are iterative algorithms that optimize each of the RIS elements alternately while fixing the other $M-1$ elements in an iterative manner until convergence is achieved. However, these methods tend to converge to local solutions. Therefore, in this paper, we focus on heuristic methods and propose an optimization method based on sigmoid filled function to optimize (10) and (11). In the next section, we show how our approach moves from one local optimum solution to a better one using the filled function.

Since only local CSIT is available to each transmitter in the distributed case, it is not feasible to maximize the sum-rate. Thus, in Section III-B, we will define $score_i$ in (17) for Tx$_i$ and formulate the optimization problem accordingly.

## III. Proposed optimization approach

### A. Centralized RIS

The idea of the filled function optimization method was originally introduced in [34] for the continuous domain. Then, [35] updated it for the discrete domain. In this paper, we use a sigmoid-based filled function and run local and global searches to optimize (10).

**Local search:** We define $\mathcal{N}(\boldsymbol{\theta})$ as the neighbors of RIS configuration $\boldsymbol{\theta}$ such that:

$$\mathcal{N}(\boldsymbol{\theta}) = \boldsymbol{\theta} \cup \{\boldsymbol{\theta} + \boldsymbol{\lambda}_m, \boldsymbol{\lambda}_m \in \mathbf{\Lambda}\}, \tag{12}$$

where $\boldsymbol{\lambda}_m$ is an $M$-length column vector with the $m^{\text{th}}$ element chosen from $\{0, \frac{2\pi}{N}, \frac{4\pi}{N}, \ldots, \frac{2\pi(N-1)}{N}\}$ and the others set to zero; further, $\mathbf{\Lambda}$ is the direction set equals to $\mathbf{\Lambda} = \{\boldsymbol{\lambda}_m, m = 1, 2, \ldots, M\}$. Here, the local search scans all neighbors of $\boldsymbol{\theta}$ to find a solution as $\boldsymbol{\theta}^* \in \mathcal{N}(\boldsymbol{\theta})$ such that $q(\boldsymbol{\theta}^*) < q(\boldsymbol{\theta})$. If we cannot find such $\boldsymbol{\theta}^*$, we call $\boldsymbol{\theta}^* = \boldsymbol{\theta}$ the local minimizer; otherwise, we consider $\boldsymbol{\theta} = \boldsymbol{\theta}^*$ and repeat the local search.

We provide Algorithm 1 to demonstrate how the local search works. We use $i_\ell^{\text{loc}}$ to denote the number of iterations to find

**Algorithm 1** Local Search

**Input:** $\boldsymbol{\theta}_\ell$, $i_{\max}^{\text{loc}}$;
**Output:** $\boldsymbol{\theta}^*$;
1: $i_\ell^{\text{loc}} = 0$; $\boldsymbol{\theta}^* = \boldsymbol{\theta}_\ell$;
2: **for** $\boldsymbol{\lambda}_m \in \mathbf{\Lambda}$ **do**
3: $\tilde{\boldsymbol{\theta}} = \boldsymbol{\theta}_\ell + \boldsymbol{\lambda}_m$;
4: **if** $q(\tilde{\boldsymbol{\theta}}) < q(\boldsymbol{\theta}^*)$ **then**
5: $\boldsymbol{\theta}^* = \tilde{\boldsymbol{\theta}}$;
6: $i_\ell^{\text{loc}} \leftarrow i_\ell^{\text{loc}} + 1$;
7: **if** $\boldsymbol{\theta}^* \neq \boldsymbol{\theta}_\ell$ and $i_\ell^{\text{loc}} \le i_{\max}^{\text{loc}}$ **then**
8: $\boldsymbol{\theta}_\ell = \boldsymbol{\theta}^*$;
9: Go to line 2;
10: **else**
11: $\boldsymbol{\theta}^*$ is the local minimizer.

the local optimizer in the $\ell^{\text{th}}$ round of using Algorithm 1. Then, we define $i_{\max}^{\text{loc}}$ as the maximum value of $i_\ell^{\text{loc}}$. Initially, we set $i_\ell^{\text{loc}} = 0$ and $\boldsymbol{\theta}^* = \boldsymbol{\theta}_\ell$, and then, in lines 2 to 5, we check all the neighbors around $\boldsymbol{\theta}_\ell$ to find a better solution than $\boldsymbol{\theta}_\ell$. To do this, we set $\tilde{\boldsymbol{\theta}} = \boldsymbol{\theta}_\ell + \boldsymbol{\lambda}_m$. If $q(\tilde{\boldsymbol{\theta}}) < q(\boldsymbol{\theta}^*)$, $\tilde{\boldsymbol{\theta}}$ offers a better solution than $\boldsymbol{\theta}^*$; hence, we set $\boldsymbol{\theta}^* = \tilde{\boldsymbol{\theta}}$. Following the completion of the search among $\boldsymbol{\theta}_\ell$'s neighbors, we increase $i_\ell^{\text{loc}}$ by one. If $\boldsymbol{\theta}^* = \boldsymbol{\theta}_\ell$ or $i_\ell^{\text{loc}} > i_{\max}^{\text{loc}}$, we consider $\boldsymbol{\theta}^*$ to be the local minimizer. Otherwise, we use $\boldsymbol{\theta}_\ell = \boldsymbol{\theta}^*$ and repeat lines 2 to 5 for all neighbors of new $\boldsymbol{\theta}_\ell$.

**Global search:** The filled function plays an essential role in the global search. In this work, we use filled function $Q_r(\boldsymbol{\theta}, \boldsymbol{\theta}^*)$ and define an auxiliary optimization problem as:

$$\min_{\boldsymbol{\theta}} Q_r(\boldsymbol{\theta}, \boldsymbol{\theta}^*) \quad \text{s.t.} \quad \boldsymbol{\theta}, \boldsymbol{\theta}^* \in \phi_N, \tag{13}$$

where $\boldsymbol{\theta}^*$ is the current local minimizer of (10), and $r > 0$ denotes the filled function parameter. The aim here is to find a better solution than $\boldsymbol{\theta}^*$. The global search begins with random configuration $\boldsymbol{\theta}_0$ and uses the local search for (10) to obtain $\boldsymbol{\theta}_0^*$ as its local minimizer. Then, to find a better solution, it exploits a sigmoid filled function, which is given by:

$$Q_r(\boldsymbol{\theta}, \boldsymbol{\theta}^*) = (1 + \frac{1}{1 + \beta||\boldsymbol{\theta} - \boldsymbol{\theta}^*||^2}) f_r(q(\boldsymbol{\theta}) - q(\boldsymbol{\theta}^*)), \tag{14}$$

where

$$f_r(q(\boldsymbol{\theta}) - q(\boldsymbol{\theta}^*)) \tag{15}$$
$$= \begin{cases} q(\boldsymbol{\theta}) - q(\boldsymbol{\theta}^*) + r, & q(\boldsymbol{\theta}) - q(\boldsymbol{\theta}^*) \leq -r, \\ \frac{1}{1 + e^{\frac{-6}{r}(q(\boldsymbol{\theta}) - q(\boldsymbol{\theta}^*) + r/2)}}, & -r < q(\boldsymbol{\theta}) - q(\boldsymbol{\theta}^*) < 0, \\ 1, & q(\boldsymbol{\theta}) - q(\boldsymbol{\theta}^*) \geq 0, \end{cases}$$

and

$$\beta = \begin{cases} 0, & q(\boldsymbol{\theta}) - q(\boldsymbol{\theta}^*) \leq -r, \\ 1, & \text{otherwise.} \end{cases} \tag{16}$$

It applies $\boldsymbol{\theta}_0^*$ to (14) and runs the local search for (13) to obtain $\tilde{\boldsymbol{\theta}}_0^*$. Next, it assumes $\boldsymbol{\theta}_1 = \tilde{\boldsymbol{\theta}}_0^*$ and runs the local search for (10) with $\boldsymbol{\theta}_1$ to attain $\boldsymbol{\theta}_1^*$ as a new local minimizer. We call $\boldsymbol{\theta}_1^*$ a better solution than the previous local minimizer if $q(\boldsymbol{\theta}_1^*) < q(\boldsymbol{\theta}_0^*)$. It repeats this procedure until a stopping criterion is satisfied. Here, we use $r$ as the optimization parameter. Intuitively, $r$ denotes a radius around $\boldsymbol{\theta}^*$ that the algorithm seeks for a new solution. If the global search fails to identify a better solution with $r$, it reduces $r$ by using $r = r/10$, resulting in a smaller search area surrounding the local minimizer. Notice that if the global search discovers a new solution, it resets $r$ to its initial value. Moreover, we use $i_m^{\text{filled}}, m = 0, 1, 2, \ldots, (N-1)M$ to denote the number of times our method searches for a new solution by scanning the $m^{\text{th}}$ neighbor of a local minimizer obtained from (13). Then, we define $i_{\max}^{\text{filled}}$ as the maximum number of times the global search uses the filled function to search for a new solution. Finally, we stop the procedure if $\sum_{m=0}^{(N-1)M} i_m^{\text{filled}} > i_{\max}^{\text{filled}}$ or $r < \epsilon$, for some $\epsilon \ll 1$ (e.g., $\epsilon = 0.01$), and declare the latest solution as the output of the global search.

Then, to accelerate the search process, in this paper, we modify the global search and use the local search to optimize (10) every $\tau \in \mathbb{N}$ times. More precisely, after $\tau$ times of finding the local minimizer of the auxiliary optimization problem, we run the local search for (10) to minimize $q(\boldsymbol{\theta})$.

We provide Algorithm 2 to describe the global search. The algorithm's inputs are $\boldsymbol{\theta}_0, r > 1, \tau \geq 1, \epsilon \ll 1, i_{\max}^{\text{loc}}$, and $i_{\max}^{\text{filled}}$, where $\boldsymbol{\theta}_0$ is selected randomly. Here, the output is $\boldsymbol{\theta}^{**}$, and we use $\ell, r_0$, and $\bar{\tau}$ to denote the $\ell^{\text{th}}$ round of the global search, to keep the initial value of $r$, and to show which round of the global search uses the local search for (10), respectively. Initially, we set $\ell = 0$, $r_0 = r$, $\bar{\tau} = \tau$, $i_m^{\text{filled}} = 0, m = 0, 1, \ldots, (N-1)M$, and $\boldsymbol{\theta}^{**} = \boldsymbol{\theta}_0$. Then, if $\ell + 1 \geq \bar{\tau}$, we update $\bar{\tau}$ and run the local search for (10) with $\boldsymbol{\theta}_\ell$ to get its local minimizer as $\boldsymbol{\theta}_\ell^*$. Otherwise, we skip the local search and consider $\boldsymbol{\theta}_\ell^* = \boldsymbol{\theta}_\ell$. Next, if $q(\boldsymbol{\theta}_\ell^*) < q(\boldsymbol{\theta}^{**})$ or $\ell = 0$, we set $\boldsymbol{\theta}_\ell^*$ as a new optimal solution, reset the value of $r$ ($r = r_0$), and put $m = 1$ where $m$ represents the index of a neighbor around $\boldsymbol{\theta}_\ell^*$. Then, we use the local search for (13) with $\boldsymbol{\theta}_\ell^*$ to obtain $\bar{\boldsymbol{\theta}}_\ell^*$ and set $i_{m-1}^{\text{filled}} \leftarrow i_{m-1}^{\text{filled}} + 1$. If $m = 1$, we increase $\ell$ by one and set $\boldsymbol{\theta}_\ell = \bar{\boldsymbol{\theta}}_{\ell-1}^*$; else, the algorithm knows that it searched at least one of the neighbors around $\boldsymbol{\theta}_\ell^*$ and put $\boldsymbol{\theta}_\ell = \bar{\boldsymbol{\theta}}_\ell^*$. Then, it goes to line 4. Thereafter, if $q(\boldsymbol{\theta}_\ell) \geq q(\boldsymbol{\theta}^{**})$, the global search checks whether it covers all the neighbors around $\boldsymbol{\theta}_\ell^*$ or not. If the answer is no, it updates $\boldsymbol{\theta}_\ell^*$, increases $m$ by one, and goes to line 12. Otherwise, if $\sum_{m=0}^{(N-1)M} i_m^{\text{filled}} > i_{\max}^{\text{filled}}$ or $r < \epsilon$, it stops the searching process and declares $\boldsymbol{\theta}^{**}$ as the global minimizer; else, it confines the searching area by reducing $r$. Then, it sets $\ell \leftarrow \ell - 1$ and goes to line 11.

**Algorithm 2** Global Search

**Input:** $\boldsymbol{\theta}_0, r, \tau, \epsilon, i_{\max}^{\text{loc}}, i_{\max}^{\text{filled}}$;
**Output:** $\boldsymbol{\theta}^{**}$;
1: $\ell = 0$; $r_0 = r$; $\bar{\tau} = \tau$;
2: $i_m^{\text{filled}} = 0$, for $m = 0, 1, \ldots, (N-1)M$;
3: $\boldsymbol{\theta}^{**} = \boldsymbol{\theta}_0$;
4: **if** $\ell + 1 \geq \bar{\tau}$ **then**
5: $\quad \bar{\tau} \leftarrow \bar{\tau} + \tau$;
6: $\quad$ Run Algo. 1 with $\boldsymbol{\theta}_\ell$ and (10) to find $\boldsymbol{\theta}_\ell^*$;
7: **else**
8: $\quad \boldsymbol{\theta}_\ell^* = \boldsymbol{\theta}_\ell$;
9: **if** $q(\boldsymbol{\theta}_\ell^*) < q(\boldsymbol{\theta}^{**})$ or $\ell = 0$ **then**
10: $\quad \boldsymbol{\theta}^{**} = \boldsymbol{\theta}_\ell^*$; $r = r_0$;
11: $\quad m = 1$;
12: $\quad$ Run Algo. 1 with $\boldsymbol{\theta}_\ell^*$ and (13) to get $\bar{\boldsymbol{\theta}}_\ell^*$;
13: $\quad i_{m-1}^{\text{filled}} \leftarrow i_{m-1}^{\text{filled}} + 1$
14: $\quad$ **if** $m = 1$ **then**
15: $\quad\quad \ell \leftarrow \ell + 1$;
16: $\quad\quad \boldsymbol{\theta}_\ell = \bar{\boldsymbol{\theta}}_{\ell-1}^*$;
17: $\quad$ **else**
18: $\quad\quad \boldsymbol{\theta}_\ell = \bar{\boldsymbol{\theta}}_\ell^*$;
19: $\quad$ Go to line 4;
20: **if** $m \leq (N-1)M$ **then**
21: $\quad \boldsymbol{\theta}_\ell^* = \boldsymbol{\theta}_{\ell-1}^* + \boldsymbol{\lambda}_m$;
22: $\quad m \leftarrow m + 1$;
23: $\quad$ Go to line 12;
24: **else**
25: $\quad$ **if** $\sum_{m=0}^{(N-1)M} i_m^{\text{filled}} > i_{\max}^{\text{filled}}$ or $r < \epsilon$ **then**
26: $\quad\quad \boldsymbol{\theta}^{**}$ is selected as global minimizer.
27: $\quad$ **else**
28: $\quad\quad r \leftarrow \frac{r}{10}$;
29: $\quad\quad \ell \leftarrow \ell - 1$;
30: $\quad\quad$ Go to line 11;

**Remark 1.** *We note that the filled function-based optimization methods can optimize a general nonlinear objective function as long as selecting a possible configuration from a discrete set is the only constraint. This model is usually referred to as an unconstrained optimization problem [35].*

According to Remark 1, we can apply our sigmoid filled function method to the max-min optimization problem in (11).

### *B. Distributed RIS*

In this case, we assume each transmitter only knows its own local CSIT; therefore, we define $score_i$ as a new objective function that captures the fact of enhancing the desired signals from $\mathsf{Tx}_i, i = 1, 2, \ldots, K$ at $\mathsf{Rx}_i$ while suppressing the

interference signals from $\mathsf{Tx}_i$ at other receivers. Consequently, we write $score_i$ as:

$$score_i \triangleq \frac{P_i\left|\mathbf{g}^{[ii]}\boldsymbol{\Theta}^{[i]}\mathbf{h}^{[ii]}+h_d^{[ii]}\right|^2}{\sigma^2+\sum_{j=1,j\neq i}^{K}P_i\left|\mathbf{g}^{[ij]}\boldsymbol{\Theta}^{[i]}\mathbf{h}^{[ii]}+h_d^{[ij]}\right|^2}, \quad (17)$$

where compared to $\text{SINR}_i$ given in (6), the denominator includes noise and the interference caused by $\mathsf{Tx}_i$ at unintended receivers. Then, we define the optimization problem for $\text{RIS}_i, 1 \leq i \leq K$, as follows:

$$\max_{\boldsymbol{\theta}^{[i]}} score_i$$
$$\text{s.t.} \quad \boldsymbol{\theta}^{[i]} = [\theta_1^{[i]}, \theta_2^{[i]}, \ldots, \theta_M^{[i]}],\ \theta_m^{[i]} \in \phi_N,\ 1 \leq m \leq M. \quad (18)$$

Here, we use the same strategy as Section III-A to maximize (18) since the filled function can be applied to a general unconstrained optimization problem.

## IV. Minimum number of required RIS elements

Prior results, for the most part, either do not consider the number of RIS elements and instead focus on adjusting the elements of a given RIS [36] or obtain the number of RIS elements at high SNRs [11]. On the contrary, in this work, we compute a lower bound on the minimum number of RIS elements to guarantee to achieve a specific value of SINR at each receiver.

### A. Centralized RIS

Usually, RIS elements are configured based on channel coefficients; however, to find a lower-bound on $M$ in this work, we assume that $\boldsymbol{\theta}$ is independent of the channels and selected randomly with uniform distribution. This assumption has been used in [37, 38] for switch-based beamforming techniques. For simplicity, we focus on a symmetric scenario, which includes the following: (i) All transmitters have the same transmit power (i.e., $P_i = P, i \in \{1, 2, , \ldots K\}$); Each receiver stands at the same distance from all transmitters; (iii) The distance between the RIS and all transmitters are the same; (iv) The receivers are placed at the same distance from the RIS. We use the following two lemmas to explain our analysis.

**Lemma 1.** *[37] If $\boldsymbol{g}^{[i]}$ shows the channel vector between RIS and $\mathsf{Rx}_i$, whose elements are independent and identically distributed (i.i.d.) random variables with zero mean and variance $\sigma_g^2$, and $\boldsymbol{h}^{[j]}$ denotes the LoS channel vector between $\mathsf{Tx}_j$ and RIS with value $m_h$. Then, for a given RIS configuration $\boldsymbol{\Theta}$, where all elements are drawn independently at random from $\{0, \frac{2\pi}{N}, \ldots, \frac{2\pi(N-1)}{N}\}$, the variance of $\boldsymbol{g}^{[i]}\boldsymbol{\Theta}\boldsymbol{h}^{[j]}$ is equal to:*

$$\nu = M\sigma_g^2(m_h)^2. \quad (19)$$

*Proof.* We have:

$$\nu = \text{var}\left(\sum_{m=1}^{M} g_m^{[i]}e^{j\theta_m}h_m^{[j]}\right) \overset{(a)}{=} \sum_{m=1}^{M}\text{var}\left(g_m^{[i]}e^{j\theta_m}\right)(m_h)^2$$
$$\overset{(b)}{=} \sum_{m=1}^{M}\left(\sigma_g^2\underbrace{\text{var}\left(e^{j\theta_m}\right)}_{1}+\sigma_g^2\underbrace{\left[\mathbb{E}\left(e^{j\theta_m}\right)\right]^2}_{=0}\right)(m_h)^2 \quad (20)$$
$$+\sum_{m=1}^{M}\underbrace{\left[\mathbb{E}\left(g_m^{[i]}\right)\right]^2}_{=0}\text{var}\left(e^{j\theta_m}\right)(m_h)^2 = M\sigma_g^2(m_h)^2,$$

where $\text{var}(X)$ denotes the variance of $X$. Here, $(a)$ holds since $h_m^{[j]}$ is constant and $e^{j\theta_m}$ and $g_m^{[i]}$ are independent. Further, $(b)$ follows the rule of the variance of the product of two independent variables. Hence, (20) completes the proof. □

**Lemma 2.** *For any $\delta_{ji} > 0, i, j \in \{1, 2, \ldots, K\}, j \neq i$,*

$$\Pr\left(\left|\boldsymbol{g}^{[i]}\boldsymbol{\Theta}\boldsymbol{h}^{[j]}\right| < \frac{\delta_{ji}}{2}\middle|\boldsymbol{\Theta}\right) > \Pr\left(\left|Re\{\boldsymbol{g}^{[i]}\boldsymbol{\Theta}\boldsymbol{h}^{[j]}\}\right| < \frac{\delta_{ji}}{2\sqrt{2}}\middle|\boldsymbol{\Theta}\right) \quad (21)$$
$$\times \Pr\left(\left|Im\{\boldsymbol{g}^{[i]}\boldsymbol{\Theta}\boldsymbol{h}^{[j]}\}\right| < \frac{\delta_{ji}}{2\sqrt{2}}\middle|\boldsymbol{\Theta}\right) \approx \left(\frac{\delta_{ji}}{\sqrt{2\pi\nu}}\right)^2.$$

*Proof.* We defer the proof to Appendix A. □

Similar to Lemma 2, for any $\delta_{ji} > 0, j \neq i$,

$$\Pr\left(\left|h_d^{[ji]}\right| < \frac{\delta_{ji}}{2}\middle|\boldsymbol{\Theta}\right) > \Pr\left(\left|Re\{h_d^{[ji]}\}\right| < \frac{\delta_{ji}}{2\sqrt{2}}\middle|\boldsymbol{\Theta}\right) \quad (22)$$
$$\times \Pr\left(\left|Im\{h_d^{[ji]}\}\right| < \frac{\delta_{ji}}{2\sqrt{2}}\middle|\boldsymbol{\Theta}\right) \approx \left(\frac{\delta_{ji}}{\sigma_{h_d}\sqrt{2\pi}}\right)^2.$$

Further, for any $\Delta_{ii} > 0$, we have:

$$\Pr\left(\left|h_d^{[ii]}\right| > \Delta_{ii}\middle|\boldsymbol{\Theta}\right) > \Pr\left(\left|Re\{h_d^{[ii]}\}\right| > \frac{\Delta_{ii}}{\sqrt{2}}\middle|\boldsymbol{\Theta}\right) \quad (23)$$
$$\times \Pr\left(\left|Im\{h_d^{[ii]}\}\right| > \frac{\Delta_{ii}}{\sqrt{2}}\middle|\boldsymbol{\Theta}\right)$$
$$= \left[2\int_{\frac{\Delta_{ii}}{\sqrt{2}}}^{\infty}\frac{1}{\sigma_{h_d}\sqrt{\pi}}e^{\frac{-r^2}{\sigma_{h_d}^2}}dr\right]^2 = \left[2Q\left(\frac{\Delta_{ii}}{\sigma_{h_d}}\right)\right]^2,$$

where $Q(.)$ represents Q-function. Finally, we present a lower bound on the minimum number of RIS elements as follows.

**Lemma 3.** *To achieve a per-user given value of SINR as $\tilde{\text{SINR}}$, the minimum number of RIS elements should follow* (24) *(on top of the next page), where $Q^{-1}(.)$ is the inverse Q-function, $\log_N$ is a logarithmic function in base $N$, $\nu' = \nu/M$, and $a$ shows a trade-off between signal enhancement from the desired transmitter and suppressing the interference signals from other transmitters. For instance, we use $a = 0$ to dedicate RIS elements to reduce the interference and $a = M$ to exploit RIS elements to improve the desired signal.*

*Proof.* Based on (6), to calculate $\text{SINR}_i$, we need to know the values of $\left|\mathbf{g}^{[i]}\boldsymbol{\Theta}\mathbf{h}^{[j]}+h_d^{[ji]}\right|$ and $\left|\mathbf{g}^{[i]}\boldsymbol{\Theta}\mathbf{h}^{[i]}+h_d^{[ii]}\right|$. Here, we aim to have $\left|\mathbf{g}^{[i]}\boldsymbol{\Theta}\mathbf{h}^{[j]}+h_d^{[ji]}\right| < \delta_{ji}$ and $\left|\mathbf{g}^{[i]}\boldsymbol{\Theta}\mathbf{h}^{[i]}+h_d^{[ii]}\right| > \Delta_{ii}$

This article has been accepted for publication in IEEE Internet of Things Journal. This is the author's version which has not been fully edited and content may change prior to final publication. Citation information: DOI 10.1109/JIOT.2023.3305914



$$M \geq \min_{a}\Big\{K^2 \log_N \Big[\frac{\tilde{\text{SINR}} 2\pi(K-1)(512\nu')}{\Big(\sigma_{h_d}\Big[Q^{-1}\big(\frac{1}{2N^{a/2K}}\big)\Big] - N^{\frac{-(10-a)}{2K^2}}\sqrt{\frac{\pi}{2}512\nu'}\Big)^2 - \frac{\tilde{\text{SINR}}\sigma^2}{P}}\Big] + a\Big\}, \tag{24}$$

at $\mathsf{Rx}_i$. For simplicity, we use $\delta_{ji} = \delta$ and $\Delta_{ii} = \Delta$. Then, we have:

$$\Big|\mathbf{g}^{[i]}\mathbf{\Theta}\mathbf{h}^{[j]} + h_d^{[ji]}\Big| \overset{(a)}{\leq} \Big|\mathbf{g}^{[i]}\mathbf{\Theta}\mathbf{h}^{[j]}\Big| + \Big|h_d^{[ji]}\Big| < \delta, \tag{25}$$

where $(a)$ follows the triangle inequality. Further, $\Big|\mathbf{g}^{[i]}\mathbf{\Theta}\mathbf{h}^{[i]} + h_d^{[ii]}\Big|$ can be lower-bounded by:

$$\Big|\mathbf{g}^{[i]}\mathbf{\Theta}\mathbf{h}^{[i]} + h_d^{[ii]}\Big| \geq \Big|h_d^{[ii]}\Big| - \Big|\mathbf{g}^{[i]}\mathbf{\Theta}\mathbf{h}^{[i]}\Big| > \Delta. \tag{26}$$

The inequalities in (25) and (26) can be met if $\Big|\mathbf{g}^{[i]}\mathbf{\Theta}\mathbf{h}^{[j]}\Big| < \delta/2$, $\Big|h_d^{[ji]}\Big| < \delta/2$, and $\Big|h_d^{[ii]}\Big| > \Delta + \delta/2$. We calculate the probability of these three events using (21), (22), and (23), respectively. In addition, there are $N^M$ different RIS configurations. Thus, to have one RIS configuration that satisfies (25) and (26) from all transmitters at all receivers, we need:

$$N^M[2Q(\frac{\Delta+\delta/2}{\sigma_{h_d}})]^{2K}(\frac{\delta}{\sqrt{2\pi M\nu'}})^{2K}(\frac{\delta}{\sigma_{h_d}\sqrt{2\pi}})^{2K(K-1)} > 1. \tag{27}$$

Without loss of generality, we assume $M\nu' \geq \sigma_{h_d}^2$, which happens if the reflected signal through the RIS is stronger than the signal from the direct path. Then, we rewrite (27) as:

$$N^M[2Q(\frac{\Delta+\delta/2}{\sigma_{h_d}})]^{2K}(\frac{\delta}{\sqrt{2\pi M\nu'}})^{2K^2} > 1. \tag{28}$$

To calculate (28), we assume:

$$\delta = N^{\frac{-(M-a)}{2K^2}}\sqrt{2\pi M^+\nu'}, \tag{29}$$

where $M^+$ is the maximum value of $M$ and $0 \leq a \leq M$ illustrates a trade-off between improving the desired signal and suppressing the interference signals. Then, by substituting $\delta$ in (28), we obtain:

$$N^a[2Q(\frac{\Delta+\delta/2}{\sigma_{h_d}})]^{2K}(\frac{M^+}{M})^{K^2} > 1, \tag{30}$$

where $(\frac{M^+}{M})^{K^2} > 1$ because $M < M^+$. Thus, we need:

$$Q(\frac{\Delta+\delta/2}{\sigma_{h_d}}) = \frac{1}{2N^{a/2K}}, \tag{31}$$

to meet the inequality in (28). As a result, we calculate $\Delta$ as:

$$\begin{aligned}\Delta &= \sigma_{h_d}\Big[Q^{-1}\big(\frac{1}{2N^{a/2K}}\big)\Big] - \frac{\delta}{2} \\ &\overset{(29)}{=} \sigma_{h_d}\Big[Q^{-1}\big(\frac{1}{2N^{a/2K}}\big)\Big] - N^{\frac{-(M-a)}{2K^2}}\sqrt{\frac{\pi}{2}M^+\nu'}.\end{aligned} \tag{32}$$

Now, we use (6) to compute SINR at $\mathsf{Rx}_i$ as below:

$$\begin{aligned}\text{SINR}_i &= \frac{P\Big|\mathbf{g}^{[i]}\mathbf{\Theta}\mathbf{h}^{[i]} + h_d^{[ii]}\Big|^2}{\sigma^2 + P\sum_{j=1,j\neq i}^{K}\Big|\mathbf{g}^{[i]}\mathbf{\Theta}\mathbf{h}^{[j]} + h_d^{[ji]}\Big|^2} \\ &\overset{(b)}{>} \frac{P\Delta^2}{\sigma^2 + P(K-1)\delta^2} \\ &= \frac{\Big(\sigma_{h_d}\Big[Q^{-1}\big(\frac{1}{2N^{a/2K}}\big)\Big] - N^{\frac{-(M-a)}{2K^2}}\sqrt{\frac{\pi}{2}M^+\nu'}\Big)^2}{\frac{\sigma^2}{P} + 2\pi(K-1)N^{\frac{-(M-a)}{K^2}}(M^+\nu')} \\ &\overset{(c)}{>} \frac{\Big(\sigma_{h_d}\Big[Q^{-1}\big(\frac{1}{2N^{a/2K}}\big)\Big] - N^{\frac{-(M^- -a)}{2K^2}}\sqrt{\frac{\pi}{2}M^+\nu'}\Big)^2}{\frac{\sigma^2}{P} + 2\pi(K-1)N^{\frac{-(M-a)}{K^2}}(M^+\nu')},\end{aligned} \tag{33}$$

where $(b)$ holds using (25) and (26), and $(c)$ is correct by assuming $M^-$ as the minimum value of $M$. Our goal is to attain a lower bound on $M$ that ensures $\text{SINR}_i > \tilde{\text{SINR}}$. To do so, the right-hand side of (33) should be greater than or equal to $\tilde{\text{SINR}}$. Consequently, we have:

$$\frac{\Big(\sigma_{h_d}\Big[Q^{-1}\big(\frac{1}{2N^{a/2K}}\big)\Big] - N^{\frac{-(M^- -a)}{2K^2}}\sqrt{\frac{\pi}{2}M^+\nu'}\Big)^2}{\frac{\sigma^2}{P} + 2\pi(K-1)N^{\frac{-(M-a)}{K^2}}(M^+\nu')} \geq \tilde{\text{SINR}}. \tag{34}$$

We note that (34) depends on the value of $a$; therefore, by taking $\log_N$ from both sides of (34) and considering $10 < M < 512$, we derive (24), which completes the proof. □

Later, in Section V, we calculate the optimal value of $a$ that maximizes the left-hand side of (34) numerically. We define $M_{\min}$ as the smallest integer that satisfies (24). Further, we refer to the curve that shows the average sum-rate versus different values of $P$ using $M_{\min}$ RIS elements as the theoretical-bound.

### *B. Distributed RIS*

In this part, we use the following lemma to show a lower bound on $M$ that guarantees achieving a given value of $score_i$ as $\tilde{score}$ in a symmetric scenario as described in Section IV-A.

**Lemma 4.** *To achieve a per-user given value of $score_i$, as $\tilde{score}$, the minimum number of RIS elements at $RIS_i$, where $10 < M < 512$, should follow* (35) *(on top of the next page).*

*Proof.* The proof is similar to Lemma 3. □

## V. Simulation results

This section includes the numerical results of our proposed method. We present the results in two parts. First, we compare distributed RISs with a centralized RIS when the channels follow the small-scale fading outlined in Section II. More

This article has been accepted for publication in IEEE Internet of Things Journal. This is the author's version which has not been fully edited and content may change prior to final publication. Citation information: DOI 10.1109/JIOT.2023.3305914



$$M > \min_{a}\Big\{(K-1)\log_N\Big[\frac{s\tilde{c}ore\frac{\pi}{2}(K-1)(\sigma_{h_d}^2+512\nu')}{(\sigma_{h_d}^2+10\nu')\Big[Q^{-1}\big(\frac{1}{2N^{a/2}}\big)\Big]^2-\frac{\sigma^2}{P}s\tilde{c}ore}\Big]+a\Big\}. \tag{35}$$

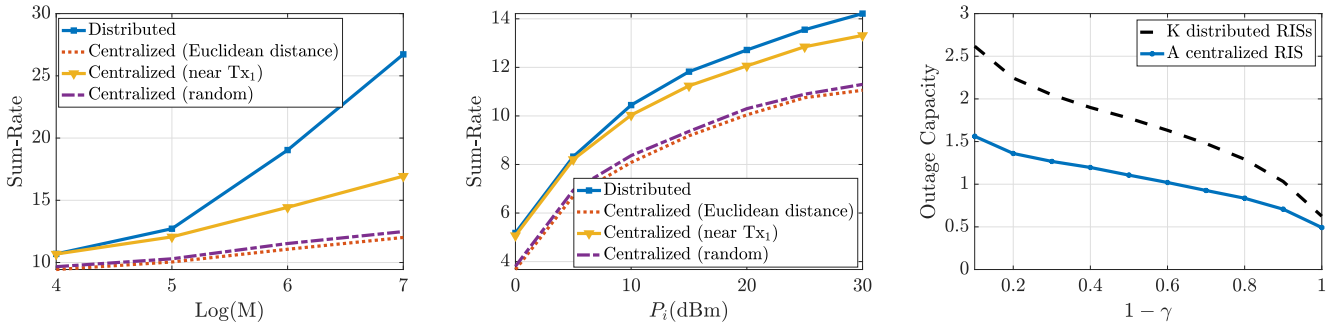


(a) (b) (c)

Fig. 2. *(a) A comparison between the distributed RIS case and three different scenarios based on the centralized RIS when $K = 4$, $P_i = 20$dB, and $M \in \{16, 32, 64, 128\}$; (b) Sum-rate versus $P_i$ using the distributed RISs and different strategies based on a centralized RIS when $K = 4$ and $M = 32$; (c) Outage capacity analysis of using a centralized RIS and $K$ distributed RISs when $K = 4$ and the channels are noiseless.*

precisely, we study the sum-rate and show the outage capacity using these two scenarios. In the second part, we assess the performance of our filled function optimization method with different benchmarks using a centralized RIS. In particular, we consider four baselines: the SES method, GA, SR [14] method, and Modified SR (M-SR) [15] method. We compare our method with them in terms of rate (sum-rate and minimum rate) and complexity when the channels between the APs and RIS are distributed based on the Rician fading model. Then, we utilize a more realistic channel model where all channels follow Nakagami fading model. Finally, we study the minimum required RIS elements to provide a certain performance with a centralized RIS.

Throughout this section, we set $\sigma^2 = -80$dBm, $\tau = 10, r = 10$, and $\epsilon = 0.01$, and we consider 3.5, 2, and 2.1 as the path loss exponents between the transmitters and the receivers, between the transmitters and the RIS(s), and between the RIS(s) and the receivers, respectively [39].

### A. Distributed RIS vs. centralized RIS

**Sum-rate analysis:** We investigate the performance of the distributed case with three distinct scenarios under the centralized case with noiseless channels. We regard $M$ as the total budget of the smart surfaces, meaning that $\text{RIS}_i, i = 1, 2, \ldots, K$ contains $\frac{M}{K}$ elements and the centralized RIS utilizes $M$ elements. Suppose $K = 4$, $N = 4$, $C_0 = -30$ dB, the transmitters are available at $(50, 0), (0, 50), (100, 50)$, and $(50, 100)$, the distributed RISs are located at $(47, 4), (3, 54), (97, 46)$, and $(53, 96)$, and the receivers are spread at random in a room of size $100 \times 100$. We assume three scenarios for the location of the centralized RIS: (1) Euclidean distance between transmitters (i.e., $(50, 50)$), (2) near one of the transmitters (e.g., close to $\mathsf{Tx}_1$ at $(47, 4)$), and (3) at random. We consider (10) and (18) as the optimization problems with a centralized RIS and the distributed RISs, respectively. In Fig. 2(a), we show sum-rate against $\log(M)$ when $P_i = 20$dBm for $i = 1, 2, \ldots, K$. As Fig. 2(a) shows, the distributed case outperforms all scenarios with a centralized

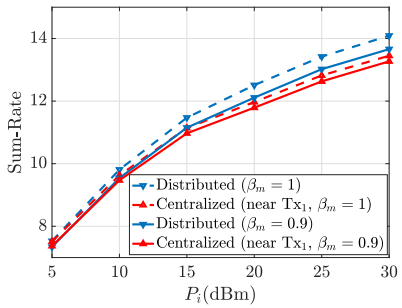


Fig. 3. *A sum-rate comparison between distributed RIS and a case with a centralized RIS, where the RIS is located near* $\mathsf{Tx}_1$ *using* $\beta_m \in \{0.9, 1\}$.

RIS and needs fewer elements to attain a given sum-rate. This occurs since determining the optimal placement of the single RIS is challenging, whereas each distributed RIS is located near its associated transmitter. In addition, in Fig. 2(b), we compare the aforementioned cases when $M = 32$, $P_i \in [0, 30]$ dBm at all transmitters, and all other assumptions are the same as in Fig. 2(a). It depicts that the distributed scenario outperforms the other cases. Moreover, Fig. 2(b) shows that the curves become saturated at high transmit power due to strong interference signals. Fig. 2(a) and (b) also illustrate that among the centralized scenarios, the case with an RIS near $\mathsf{Tx}_1$ outperforms the others, while the Euclidean case performs the poorest. Here, the RIS near $\mathsf{Tx}_1$ focuses on $\mathsf{Rx}_1$, potentially sacrificing fairness for a higher sum-rate. Conversely, the Euclidean case aims to maximize sum-rate while maintaining fairness, which poses challenges. The random case falls between these scenarios, prioritizing a given user if the RIS is randomly close to the transmitter corresponding to that user and resembling the Euclidean case when RIS is positioned far from all transmitters. Thus, the random case slightly outperforms the Euclidean case, albeit remaining close to the Euclidean case, due to the lower probability of RIS proximity to any transmitter.

**Outage capacity analysis:** In this work, we mainly focus on the average rates. However, from a practical standpoint, it

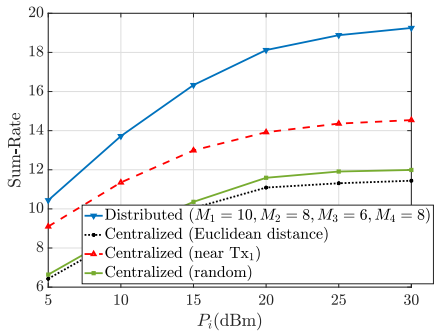


Fig. 4. *Sum-rate against $P_i$ using distributed RISs, where each RIS has a different number of elements, and three cases based on centralized RIS.*

is important to understand the outage probability resulting in failure to achieve target rates. Thus, we study the RIS-assisted networks' outage capacity with distributed and centralized RISs under noiseless channels. We define $(1-\gamma)$ outage capacity for the $i^{\text{th}}$ user, $i \in \{1, 2, \ldots, K\}$ as:

$$C_i^{1-\gamma} = \{R_i : \Pr(R_i \geq R_0) \geq 1-\gamma\}, \tag{36}$$

where $R_i$ shows the rate for the $i^{\text{th}}$ user in which there exists a configuration at RIS(s) with channel capacity more than or equal to $R_0$ with a probability greater than or equal to $1-\gamma$. Fig. 2(c) shows the outage capacity of the centralized and distributed scenarios. In the centralized case, we assume 50, 5, and 47.17 represent the distance between $\mathsf{Tx}_i$ and $\mathsf{Rx}_j, i, j \in \{1, 2, 3, 4\}$, the distance between $\mathsf{Tx}_i$ and the RIS, and the distance between the RIS and $\mathsf{Rx}_j$, respectively. Then, in the distributed case, we consider the RISs are located at $(25, 25), (25, 75), (75, 75)$, and $(75, 25)$. Here, we assume other assumptions are analogous to Fig. 2(b). Fig. 2(c) shows that the distributed case provides a higher outage capacity than the centralized case, which confirms the conclusions in Fig. 2(a) and Fig. 2(b) that the distributed scenario outperforms the centralized scenario.

Then, we study two practical assumptions regarding RIS elements with imperfect reflection and distributed RISs with different numbers of elements in Fig. 3 and Fig. 4, respectively. Specifically, Fig. 3 assumes a case where $\beta_m = 0.9 < 1$, and the other assumptions are similar to Fig. 2(b). We compare its performance to the case with $\beta_m = 1$. Fig. 3 shows that distributed RISs provide a higher gain than centralized RIS. Further, Fig. 3 depicts a small performance degradation when we use $\beta_m = 0.9$ since the receivers get a slightly weaker signal via the transmitter-RIS-receiver link. Next, in Fig. 4, we focus on a case where each distributed RIS utilizes a different number of elements, $\mathbf{h}^{[jj]}$ is distributed based on Rician fading with $\kappa$ (Rician factor) equals 2, and other assumptions are similar to Fig. 2(b). Here, Fig. 4 presents a sum-rate comparison between the distributed and centralized cases, considering a total budget of 32 RIS elements. In the distributed case, we select $M_1 = 10, M_2 = 8, M_3 = 6$, and $M_4 = 8$, where $M_i, 1 \leq i \leq 4$ denotes the number of elements at $\mathrm{RIS}_i$. This configuration results in a higher gain than the other cases with a centralized RIS. As observed, Fig. 3 and Fig. 4 convey a similar message to the scenario where $\beta_m = 1$ and distributed RISs have an equal number of elements. This similarity arises because the main reason for achieving better performance in the distributed scenario is that the centralized case falls short of determining the optimal RIS location, whereas each distributed RIS is positioned near its associated transmitter.

### *B. Efficiency of our optimization method*

In [14, 15], the authors propose two SR-based optimization methods, which optimize the RIS elements in an iterative fashion. In this part, we compare our filled function method with these baselines in terms of sum-rate, minimum rate (min rate), and complexity. Furthermore, since the optimization problems in (10) and (11) are NP-hard problems, it is fair to utilize two other benchmarks based on heuristic optimization methods as the SES method and GA. Here, we focus on the centralized scenario and assume that $\mathbf{h}^{[ij]}$ is distributed via Rician fading with $\kappa = 2$, and the other channels follow Rayleigh fading.

**Sum-rate:** In Fig. 5(a), we assume $K = 4$, $N = 4$, and $P_i = 20$dBm for $i = 1, 2, \ldots, K$. We also consider the channels are noiseless, $M \in \{8, 16, 32, 64, 96\}$, $C_0 = -30$ dB, and $(0, 0)$, $(50, 0)$, and $(3, 4)$ show the locations of the APs, receivers, and RIS, respectively. Fig. 5(a) shows that our approach outperforms the SR-based methods as well as two heuristic optimization methods. Further, we consider a baseline with no RIS, referred to as "No RIS-$K$ parallel channels," where all transmitters send their signals simultaneously and each transmitter delivers its message to its desired receiver with no interference. Fig. 5(a) shows that our method offers a higher sum-rate than this baseline when $M = 96$. The gap between our approach and the benchmarks grows as $M$ increases since our approach finds an approximate global solution by moving from one local optimum solution to another better one while the others get stuck in the local minimizers. Then, in Fig. 5(b), we present the sum-rate of our approach and the SR method using both noisy and noiseless channels. It depicts that our optimization approach offers acceptable sum-rate values using noisy-30 and noisy-20 channels; however, it fails to perform well when we utilize noisy-10 and noisy-0 channels. It occurs because, as the noise power in the noisy CSI grows, the impact of using more RIS elements diminishes since the actual CSI is substantially different from the noisy CSI used in the optimization process.

**Min-rate:** We focus on the max-min optimization problem in (11) to compute the min rate. The assumptions are analogous to those in Fig. 5(a). As shown in Fig. 5(c), our approach provides appreciable gains over the SR-based methods as well as GA and the SES approach due to its more efficient optimization technique. Additionally, when $M = 64$, Fig. 5(c) indicates that our approach achieves a higher min rate than the No RIS-$K$ parallel channels.

**Complexity:** In this part, we compute the complexity of our approach, the brute force search, and the baselines described in Fig. 5(a). We use the number of evaluations required to obtain the solution as a proxy for complexity, which can be derived as (37) (on top of this page), where $(a)$ happens since $i_\ell^{\text{loc}} \leq i_{\max}^{\text{loc}}$ and $\sum_{m=0}^{(N-1)M} i_m^{\text{filled}} \leq i_{\max}^{\text{filled}}$, and $(b)$ and $(c)$

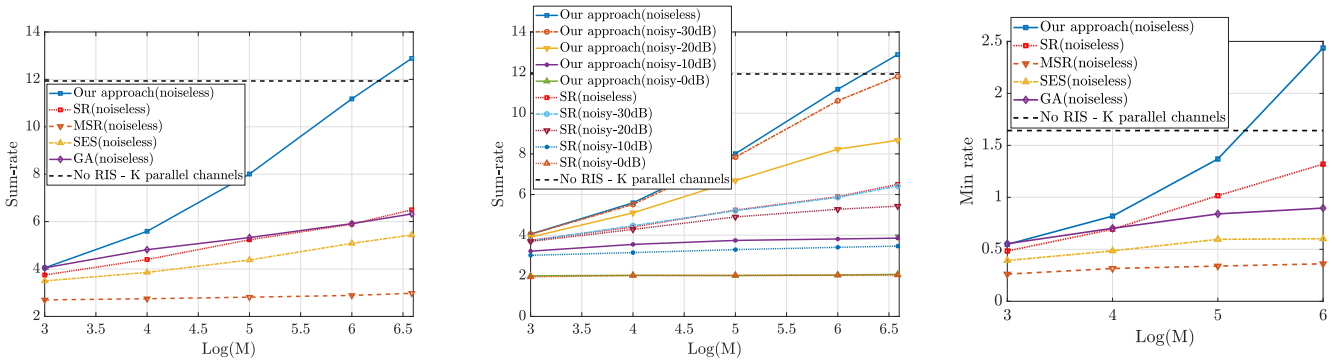


(a) (b) (c)

Fig. 5. *(a) Sum-rate against* $\log(M)$ *of our approach, the SR, M-SR, and SES methods, GA, and No RIS - K parallel channels under noiseless channels when* $K = 4$ *and* $N = 4$*; (b) Sum-rate versus different values of* $M$ *using our approach and the SR method with different versions of the noisy channels; (c) Min rate versus* $\log(M)$ *of our approach, the SR method, the M-SR method, the SES method, GA, and No RIS - K parallel channels under noiseless channels.*

$$(N-1)\,M i_0^{\text{loc}} + \sum_{m=0}^{(N-1)M} \left( \frac{(N-1)\,M i_\ell^{\text{loc}}}{\tau} + (N-1)\,M i_\ell^{\text{loc}} \right) i_m^{\text{filled}} \overset{(a)}{\leq} (N-1)\,M i_{\max}^{\text{loc}} + \frac{\tau+1}{\tau}\,(N-1)\,M i_{\max}^{\text{loc}} i_{\max}^{\text{filled}}$$
$$\overset{(b)}{\leq} (N-1)\,M i_{\max}^{\text{loc}} + \frac{\tau+1}{\tau} N\,(N-1)\,M\,((N-1)M+1)\,[\log_{10}(r/\epsilon)+1]\,i_{\max}^{\text{loc}} \overset{(c)}{\equiv} \mathcal{O}\left(N\,(N-1)^2 \log_{10}(r/\epsilon) M^3\right), \quad (37)$$

TABLE II
THE COMPLEXITY OF OUR APPROACH, BRUTE FORCE SEARCH, AND THE BENCHMARKS MENTIONED IN SECTION V-B.

| Method | $M = 32$ | $M = 64$ | Method | $M = 32$ | $M = 64$ |
|---|---|---|---|---|---|
| Brute force | $1.84 \times 10^{19}$ | $3.40 \times 10^{38}$ | SR method | $2.34 \times 10^{4}$ | $4.71 \times 10^{4}$ |
| M-SR method | $1.28 \times 10^{4}$ | $2.56 \times 10^{4}$ | Genetic algorithm | $2.01 \times 10^{4}$ | $2.01 \times 10^{4}$ |
| Simplified exhaustive search | $3.17 \times 10^{5}$ | $2.67 \times 10^{6}$ | **Sigmoid filled function** | $3.63 \times 10^{5}$ | $1.45 \times 10^{6}$ |

follow the definition of Algorithms 1 (line 7) and 2 (line 25) where $i_{\max}^{\text{loc}}$ and $i_{\max}^{\text{filled}}$ cannot be greater than $M$ and $N\,((N-1)M+1)\,[\log_{10}(r/\epsilon)+1]$, respectively. In (37), we use the Landau notation ("big O") in its standard form, and $\log_{10}$ is the logarithmic function in base 10. We use the same assumptions as in Fig. 5(a) and calculate the complexity of our method, the brute force search, the SR-based methods, GA, and the SES method when $M \in \{32, 64\}$ as Table II. This table shows that our method is faster than the brute-force search and the SES method but slower than the others, revealing the rate-complexity trade-off of the methods. Here, Table II supports the analytical complexity statement in (37).

In this work, we aim to attain the optimal RIS configuration with negligible overhead. For instance, at carrier frequency $f_c = 1.8$GHz and at the speed of $v = 60$km/h, the channel coherence time is equal to $c/(f_c v) = 10$msec, where $c$ denotes the speed of light. According to Table II, our method requires $1.45\times10^6$ evaluations to find the optimal solution with $M = 64$, and if we assume a dual-core processor with a clock frequency of 2 GHz, our approach requires approximately $0.36$msec to get the results, which is negligible.

### C. Nakagami channel model

In this part, we use a more realistic channel model based on Nakagami distribution [40]. Specifically, we define $h_m^{[j]} = |h_m^{[j]}| e^{j\bar{\theta}_{h,m}^{[j]}}$, $g_m^{[i]} = |g_m^{[i]}| e^{j\bar{\theta}_{g,m}^{[i]}}$, and $h_d^{[ji]} = |h_d^{[ji]}| e^{j\bar{\theta}_d^{[ji]}}$ as the communication channels, where $\bar{\theta}_{h,m}^{[j]}$, $\bar{\theta}_{g,m}^{[i]}$, and $\bar{\theta}_d^{[ji]}$ describe the angles of $h_m^{[j]}$, $g_m^{[i]}$, and $h_d^{[ji]}$, respectively. Here, $|h_m^{[j]}|$, $|g_m^{[i]}|$, and $|h_d^{[ji]}|$ follow a Nakagami distribution with parameters $(m_{h_m^{[j]}}, \Omega_{h_m^{[j]}})$, $(m_{h_m^{[i]}}, \Omega_{g_m^{[i]}})$, and $(m_{h_d^{[ji]}}, \Omega_{h_d^{[ji]}})$, respectively, where $\Omega$ parameters represent the large scale fading of the channels. Moreover, the angles of the channels follow independent uniform distributions. We use the cosine law to take the angle of the incident and the reflected signals at RIS into consideration. More precisely, we utilize (38) (on top of the next page) to compute $d_{\mathsf{Tx}_i-\mathsf{Rx}_i}$, where $d_{\mathsf{Tx}_i-\text{RIS}^{[m]}}$, $d_{\text{RIS}^{[m]}-\mathsf{Rx}_i}$, and $d_{\mathsf{Tx}_i-\mathsf{Rx}_i}$ indicate the distance between $\mathsf{Tx}_i$ and the $m^{\text{th}}$ element of the RIS, between the $m^{\text{th}}$ element of the RIS and $\mathsf{Rx}_i$, and between $\mathsf{Tx}_i$ and $\mathsf{Rx}_i$, respectively. We use $\psi_m$ to denote the angle between the $\mathsf{Tx}_i - \text{RIS}^{[m]}$ and $\text{RIS}^{[m]} - \mathsf{Rx}_i$ links. Fig. 6(a) depicts the comparison results between our approach and two SR-based methods using a centralized RIS when the channels are noiseless, $K = 4$, $N = 4$, and $P_i = 20$dBm for $i = 1, 2, \ldots, K$. We assume $M \in \{8, 16, 32, 64\}$, $m_{h_d^{[ji]}} = 3$, $m_{h_m^{[j]}} = 1.5$, $m_{g_m^{[i]}} = 2.5$, $\psi_m = 86°$, $C_0 = -31.5$dB, and $(0, 0)$, $(50, 0)$, and $(3, 4)$ are the locations of the APs, receivers, and RIS, respectively. According to Fig. 6(a), our filled function-based method provides a higher sum-rate than the other baselines due to finding the approximation of the global solutions instead of the local optimal solutions.

### D. Minimum required RIS elements

In this section, we analyze the minimum number of required RIS elements to obtain a desired performance metric. In particular, we focus on the following cases.

$$d_{\mathsf{Tx}_i-\mathsf{Rx}_i} = \sqrt{d^2_{\mathsf{Tx}_i-\mathsf{RIS}^{[m]}} + d^2_{\mathsf{RIS}^{[m]}-\mathsf{Rx}_i} - 2d_{\mathsf{Tx}_i-\mathsf{RIS}^{[m]}} d_{\mathsf{RIS}^{[m]}-\mathsf{Rx}_i} \cos(\psi_m)}, \tag{38}$$

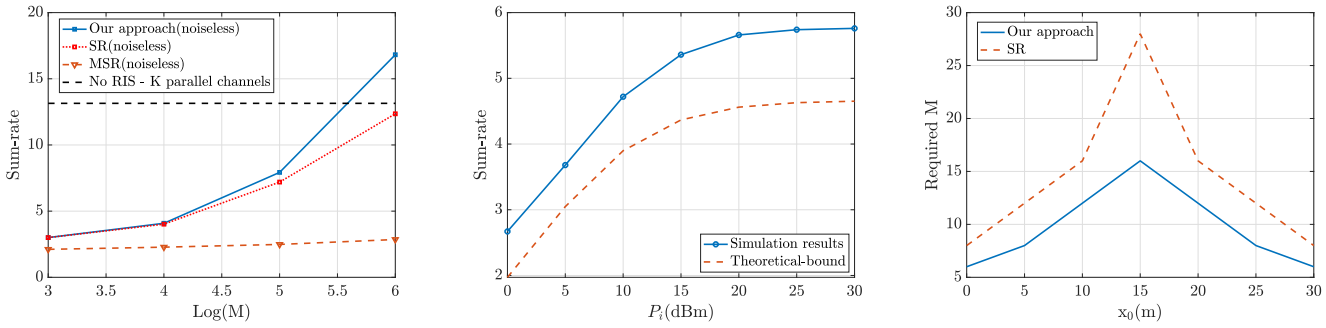


(a) (b) (c)

Fig. 6. *(a) A comparison between our approach, the SR method, and the M-SR method using Nakagami fading when $K = 4$, and $M \in \{8, 16, 32, 64\}$; (b) A comparison between our approach and the theoretical-bound with a centralized RIS when $M_{\min} = 24$, $K = 3$; (c) The number of required RIS elements to have the sum-rate of 4 with one RIS when $P_i = 30$dBm, $K = 4$, and the channels are noisy-30.*

**Theoretical lower-bound:** We assume a centralized RIS with noiseless channels and consider a symmetric setting where $K = 3$, $N = 8$, the path loss exponent between each pair of transmitter-receiver is equal to 3.9, the distance between each pair of transmitter-receiver, the distance between each transmitter and the RIS and the distance between the RIS and each receiver are equal to 25, $\sqrt{2}$, and 24.02, respectively. To obtain an accurate curve, we solve (24) numerically without utilizing the practical interval for $M$. In Fig. 6(b), we plot sum-rate versus $P_i$ with the theoretical-bound and our approach when $M_{\min} = 24$. The results show that our method provides higher results than the theoretical-bound since we obtain the theoretical-bound pessimistically (i.e., the RIS configurations are independent of the channels).

**RIS at different locations:** To study the optimal placement of the RIS, we calculate the minimum number of the RIS elements that our method and the SR method require to provide a certain sum-rate when the locations of $\mathsf{Tx}_i$, the RIS, and $\mathsf{Rx}_i$ are equal to $(0, 0)$, $(x_0, 1), x_0 \in [0, 30]$, and $(30, 0)$, respectively. Moreover, we assume a symmetric setting with a centralized RIS where $P_i = 30$dBm, the channels are noisy-30, $K = 4$, $N = 4$, and $C_0 = -30$ dB. Then, we compute the number of required RIS elements to achieve a sum-rate of 4 as described in Fig. 6(c). Not surprisingly, due to the significant product-path loss, the number of required elements is highest when the RIS is placed in the middle between the transmitters and receivers, and the RIS needs fewer elements as it moves closer to either the transmitters or the receivers. Fig. 6(c) also describes that our method requires fewer elements than the SR method due to its better optimization performance.

## VI. Conclusion

In this paper, we investigated a SISO RIS-assisted IoT network under (1) centralized RIS and (2) distributed RISs, with one RIS dedicated to each transmitter. The simulation results demonstrated that the distributed scenario offers a higher sum-rate than the centralized case and requires fewer RIS elements to provide the same performance. We proposed an optimization approach based on a sigmoid filled function to optimize the RIS elements in the discrete domain. We showed that our optimization approach provides a higher rate and requires fewer RIS elements to meet a certain sum-rate, compared to the SR-based methods [14, 15], GA, and SES methods. Finally, we evaluated the minimum required RIS elements to obtain a desired performance metric. A future direction for this work would assume a wider range for the number of distributed RISs. The main challenges are the placement of the RIS and pairing them with the transmitters.

## Acknowledgment

The work of S. Nassirpour and A. Vahid was in part supported by National Science Foundation (NSF) grants ECCS-2030285, CNS-2106692, and CNS-2211804. The work of D. Bharadia was partly supported by NSF grants CNS-2211805 and CNS-2107613.

## Appendix A
## Proof of Lemma 2

*Proof.* For a given $\boldsymbol{\Theta}$, we have a lower-bound for $\Pr\left(\left|\mathbf{g}^{[i]}\boldsymbol{\Theta}\mathbf{h}^{[j]}\right| < \frac{\delta_{ji}}{2}\middle|\boldsymbol{\Theta}\right)$ as (39), where to simplify its right-hand side, we need to show that $\left|Re\{\mathbf{g}^{[i]}\boldsymbol{\Theta}\mathbf{h}^{[j]}\}\right|$ and $\left|Im\{\mathbf{g}^{[i]}\boldsymbol{\Theta}\mathbf{h}^{[j]}\}\right|$ are independent. Notice that the independence of the real and imaginary parts of $\mathbf{g}^{[i]}\boldsymbol{\Theta}\mathbf{h}^{[j]}$ leads to the independence of $\left|Re\{\mathbf{g}^{[i]}\boldsymbol{\Theta}\mathbf{h}^{[j]}\}\right|$ and $\left|Im\{\mathbf{g}^{[i]}\boldsymbol{\Theta}\mathbf{h}^{[j]}\}\right|$. Based on Lemma 1, $Re\{\mathbf{g}^{[i]}\boldsymbol{\Theta}\mathbf{h}^{[j]}\}$ and $Im\{\mathbf{g}^{[i]}\boldsymbol{\Theta}\mathbf{h}^{[j]}\}$ are distributed via zero-mean Gaussian distribution; therefore, $Re\{\mathbf{g}^{[i]}\boldsymbol{\Theta}\mathbf{h}^{[j]}\}$ and $Im\{\mathbf{g}^{[i]}\boldsymbol{\Theta}\mathbf{h}^{[j]}\}$ are independent if they are uncorrelated (i.e., their covariance is equal to zero), which is straightforward.

Then, for $i, j \in \{1, 2, \ldots, K\}, j \neq i$, we simplify (39) as:

$$\Pr\left(\left|\mathbf{g}^{[i]}\boldsymbol{\Theta}\mathbf{h}^{[j]}\right| < \frac{\delta_{ji}}{2}\middle|\boldsymbol{\Theta}\right) > \Pr\left(\left|Re\{\mathbf{g}^{[i]}\boldsymbol{\Theta}\mathbf{h}^{[j]}\}\right| < \frac{\delta_{ji}}{2\sqrt{2}}\middle|\boldsymbol{\Theta}\right) \times \Pr\left(\left|Im\{\mathbf{g}^{[i]}\boldsymbol{\Theta}\mathbf{h}^{[j]}\}\right| < \frac{\delta_{ji}}{2\sqrt{2}}\middle|\boldsymbol{\Theta}\right). \tag{40}$$

This article has been accepted for publication in IEEE Internet of Things Journal. This is the author's version which has not been fully edited and content may change prior to final publication. Citation information: DOI 10.1109/JIOT.2023.3305914



$$\Pr\left(\left|\mathbf{g}^{[i]}\mathbf{\Theta}\mathbf{h}^{[j]}\right| < \frac{\delta_{ji}}{2}\middle|\mathbf{\Theta}\right) > \Pr\left(\left|Re\{\mathbf{g}^{[i]}\mathbf{\Theta}\mathbf{h}^{[j]}\}\right| < \frac{\delta_{ji}}{2\sqrt{2}}\middle|\mathbf{\Theta}\bigcap\left|Im\{\mathbf{g}^{[i]}\mathbf{\Theta}\mathbf{h}^{[j]}\}\right| < \frac{\delta_{ji}}{2\sqrt{2}}\middle|\mathbf{\Theta}\right), \tag{39}$$

Since $Re\{\mathbf{g}^{[i]}\mathbf{\Theta}\mathbf{h}^{[j]}\}$ is a zero-mean Gaussian random variable, for $i,j \in \{1,2,\ldots,K\}, j \neq i$, we have:

$$\begin{aligned}\Pr\left(\left|Re\{\mathbf{g}^{[i]}\mathbf{\Theta}\mathbf{h}^{[j]}\}\right| < \frac{\delta_{ji}}{2\sqrt{2}}\middle|\mathbf{\Theta}\right) &= \int_{-\frac{\delta_{ji}}{2\sqrt{2}}}^{\frac{\delta_{ji}}{2\sqrt{2}}} \frac{1}{\sqrt{\pi\nu}} e^{\frac{-r^2}{\nu}} dr \\ &\overset{(a)}{\approx} \int_{-\frac{\delta_{ji}}{2\sqrt{2}}}^{\frac{\delta_{ji}}{2\sqrt{2}}} \frac{1}{\sqrt{\pi\nu}}\Big[1 - \frac{r^2}{\nu} + O(\frac{r^4}{\nu^2})\Big] dr \\ &= \frac{1}{\sqrt{\pi\nu}}\Big[\frac{\delta_{ji}}{\sqrt{2}} - \frac{\delta_{ji}^3}{24\sqrt{2}\nu} + O(\frac{\delta_{ji}^5}{\nu^2})\Big] \overset{(b)}{\approx} \frac{\delta_{ji}}{\sqrt{2\pi\nu}}, \end{aligned} \tag{41}$$

where $(a)$ applies based on approximation from the Taylor expansion of $e^{\frac{-r^2}{\nu}}$, and $(b)$ holds since our goal is to have a small $\delta_{ji}$; therefore, we ignore the high orders of $\frac{\delta_{ji}}{\nu}$.

Similarly, for $i,j \in \{1,2,\ldots,K\}, j \neq i$, we obtain:

$$\Pr\left(\left|Im\{\mathbf{g}^{[i]}\mathbf{\Theta}\mathbf{h}^{[j]}\}\right| < \frac{\delta_{ji}}{2\sqrt{2}}\middle|\mathbf{\Theta}\right) \approx \frac{\delta_{ji}}{\sqrt{2\pi\nu}}. \tag{42}$$

Hence, using (41) and (42) leads to

$$\Pr\left(\left|\mathbf{g}^{[i]}\mathbf{\Theta}\mathbf{h}^{[j]}\right| < \frac{\delta_{ji}}{2}\middle|\mathbf{\Theta}\right) > (\frac{\delta_{ji}}{\sqrt{2\pi\nu}})^2, \tag{43}$$

which holds true for $i,j \in \{1,2,\ldots,K\}, j \neq i$, and this completes the proof. □

## REFERENCES


[1] M. Mozaffari, W. Saad, M. Bennis, and M. Debbah, "Mobile unmanned aerial vehicles (UAVs) for energy-efficient Internet of Things communications," *IEEE Transactions on Wireless Communications*, vol. 16, no. 11, pp. 7574–7589, 2017.

[2] C. V. N. Index, "Global mobile data traffic forecast update, 2017–2022," *Cisco white paper*, 2019.

[3] G. Gui, M. Liu, F. Tang, N. Kato, and F. Adachi, "6G: opening new horizons for integration of comfort, security, and intelligence," *IEEE Wireless Communications*, vol. 27, no. 5, pp. 126–132, 2020.

[4] Z. Wang, Y. Shi, Y. Zhou, H. Zhou, and N. Zhang, "Wireless-powered over-the-air computation in intelligent reflecting surface-aided IoT networks," *IEEE Internet of Things Journal*, vol. 8, no. 3, pp. 1585–1598, 2020.

[5] H. Niu, Z. Lin, Z. Chu, Z. Zhu, P. Xiao, H. X. Nguyen, I. Lee, and N. Al-Dhahir, "Joint beamforming design for secure RIS-assisted IoT networks," *IEEE Internet of Things Journal*, 2022.

[6] A. Ranjha and G. Kaddoum, "URLLC facilitated by mobile UAV relay and RIS: A joint design of passive beamforming, blocklength, and UAV positioning," *IEEE Internet of Things Journal*, vol. 8, no. 6, pp. 4618–4627, 2020.

[7] Y. Zheng, S. Bi, Y.-J. A. Zhang, X. Lin, and H. Wang, "Joint beamforming and power control for throughput maximization in IRS-assisted MISO WPCNs," *IEEE Internet of Things Journal*, vol. 8, no. 10, pp. 8399–8410, 2020.

[8] X. Li, C. Zhang, C. He, G. Chen, and J. A. Chambers, "Sum-rate maximization in IRS-assisted wireless power communication networks," *IEEE Internet of Things Journal*, vol. 8, no. 19, pp. 14959–14970, 2021.

[9] H. Xie, J. Xu, and Y.-F. Liu, "Max-min fairness in IRS-aided multi-cell MISO systems with joint transmit and reflective beamforming," *IEEE Transactions on Wireless Communications*, vol. 20, no. 2, pp. 1379–1393, 2020.

[10] M. Fu, Y. Zhou, and Y. Shi, "Reconfigurable intelligent surface for interference alignment in MIMO device-to-device networks," in *2021 IEEE International Conference on Communications Workshops (ICC Workshops)*, pp. 1–6, IEEE, 2021.

[11] A. H. A. Bafghi, V. Jamali, M. Nasiri-Kenari, and R. Schober, "Degrees of freedom of the $K$-user interference channel assisted by active and passive IRSs," *IEEE Transactions on Communications*, 2022.

[12] Y. Ni, Y. Liu, J. Wang, Q. Wang, H. Zhao, and H. Zhu, "Performance analysis for RIS-assisted D2D communication under Nakagami-$m$ fading," *IEEE Transactions on Vehicular Technology*, vol. 70, no. 6, pp. 5865–5879, 2021.

[13] C. Huang, B. Sun, W. Pan, J. Cui, X. Wu, and X. Luo, "Dynamical beam manipulation based on 2-bit digitally-controlled coding metasurface," *Scientific reports*, vol. 7, no. 1, pp. 1–8, 2017.

[14] S. Gong, Z. Yang, C. Xing, J. An, and L. Hanzo, "Beamforming optimization for intelligent reflecting surface-aided SWIPT IoT networks relying on discrete phase shifts," *IEEE Internet of Things Journal*, vol. 8, no. 10, pp. 8585–8602, 2020.

[15] Z. Abdullah, G. Chen, S. Lambotharan, and J. Chambers, "Low-complexity antenna selection and discrete phase-shifts design in IRS-assisted multiuser massive MIMO networks," *IEEE Transactions on Vehicular Technology*, 2022.

[16] B. Zheng, C. You, and R. Zhang, "Double-IRS assisted multi-user MIMO: Cooperative passive beamforming design," *IEEE Transactions on Wireless Communications*, vol. 20, no. 7, pp. 4513–4526, 2021.

[17] T. N. Do, G. Kaddoum, T. L. Nguyen, D. B. Da Costa, and Z. J. Haas, "Multi-RIS-aided wireless systems: Statistical characterization and performance analysis," *IEEE Transactions on Communications*, vol. 69, no. 12, pp. 8641–8658, 2021.

[18] S. Yang, J. Zhang, W. Xia, Y. Ren, H. Yin, and H. Zhu, "On the discrete phase shifts design for distributed RIS-aided downlink MIMO-NOMA systems," in *2022 IEEE Wireless Communications and Networking Conference (WCNC)*, pp. 363–368, IEEE, 2022.

[19] D. L. Galappaththige, D. Kudathanthirige, G. Amarasuriya, and C. Tellambura, "Weighted sum-rate maximization for distributed RIS-assisted cell-free massive MIMO," in *2022 IEEE Conference on Standards for Communications and Networking (CSCN)*, pp. 236–241, IEEE, 2022.

[20] W. Mei and R. Zhang, "Multi-beam multi-hop routing for intelligent reflecting surfaces aided massive MIMO," *IEEE Transactions on Wireless Communications*, vol. 21, no. 3, pp. 1897–1912, 2021.

[21] G. Yu, X. Chen, C. Zhong, D. W. K. Ng, and Z. Zhang, "Design, analysis, and optimization of a large intelligent reflecting surface-aided B5G cellular Internet of Things," *IEEE Internet of Things Journal*, vol. 7, no. 9, pp. 8902–8916, 2020.

[22] Q. Wu and R. Zhang, "Towards smart and reconfigurable environment: Intelligent reflecting surface aided wireless network," *IEEE Communications Magazine*, vol. 58, no. 1, pp. 106–112, 2019.

[23] A. Papazafeiropoulos, C. Pan, A. Elbir, V. Nguyen, P. Kourtessis, and S. Chatzinotas, "Asymptotic analysis of max-min weighted SINR for IRS-assisted MISO systems with hardware impairments," *IEEE Wireless Communications Letters*, 2021.

[24] Q. Wu and R. Zhang, "Intelligent reflecting surface enhanced wireless network: Joint active and passive beamforming design," in *2018 IEEE Global Communications Conference (GLOBECOM)*, pp. 1–6, IEEE, 2018.

[25] A. Vahid, V. Aggarwal, A. S. Avestimehr, and A. Sabharwal, "On the capacity of multi-hop wireless networks with partial network knowledge," in *2010 48th Annual Allerton Conference on Communication, Control, and Computing (Allerton)*, pp. 1030–1037, IEEE, 2010.

[26] A. Vahid and R. Calderbank, "Impact of local delayed CSIT on the capacity region of the two-user interference channel," in *2015 IEEE International Symposium on Information Theory (ISIT)*, pp. 2421–2425, IEEE, 2015.

[27] A. Vahid and R. Calderbank, "Two-user erasure interference channels with local delayed CSIT," *IEEE Transactions on Information Theory*, vol. 62, no. 9, pp. 4910–4923, 2016.

[28] A. Vahid, V. Aggarwal, A. S. Avestimehr, and A. Sabharwal, "Interference management with mismatched partial channel state information," *EURASIP Journal on Wireless Communications and Networking*, vol. 2017, no. 1, pp. 1–22, 2017.

[29] S. Nassirpour and A. Vahid, "On the stability region of intermittent interference networks," *IEEE Transactions on Communications*, vol. 69, no. 11, pp. 7335–7349, 2021.

[30] S. Nassirpour and A. Vahid, "Throughput, delay, and complexity trade-

offs in interference channels," in *2020 10th Annual Computing and Communication Workshop and Conference (CCWC)*, pp. 0348–0354, IEEE, 2020.
[31] A. Vahid, S.-C. Lin, and I.-H. Wang, "Erasure broadcast channels with intermittent feedback," *IEEE Transactions on Communications*, vol. 69, no. 11, pp. 7363–7375, 2021.
[32] S.-C. Lin, I.-H. Wang, and A. Vahid, "Capacity of broadcast packet erasure channels with single-user delayed CSI," *IEEE Transactions on Information Theory*, vol. 67, no. 10, pp. 6283–6295, 2021.
[33] M. Grant, S. Boyd, and Y. Y. Cvx, "Matlab software for disciplined convex programming, version 1.21," *CVX Research*, 2011.
[34] R. GE, "A filled function method for finding a global minimizer of a function of several variables," *Mathematical programming*, vol. 46, no. 1, pp. 191–204, 1990.
[35] C.-K. Ng, L.-S. Zhang, D. Li, and W.-W. Tian, "Discrete filled function method for discrete global optimization," *Computational Optimization and Applications*, vol. 31, no. 1, pp. 87–115, 2005.
[36] M. Dunna, C. Zhang, D. Sievenpiper, and D. Bharadia, "ScatterMIMO: Enabling virtual MIMO with smart surfaces," in *Proceedings of the 26th Annual International Conference on Mobile Computing and Networking*, pp. 1–14, 2020.
[37] M. Johnny and A. Vahid, "Low-complexity blind interference suppression with reconfigurable antennas," *IEEE Transactions on Wireless Communications*, vol. 21, no. 4, pp. 2757–2768, 2021.
[38] S. Nassirpour, A. Gupta, A. Vahid, and D. Bharadia, "Power-efficient analog front-end interference suppression with binary antennas," *IEEE Transactions on Wireless Communications*, 2022.
[39] Q. Wu and R. Zhang, "Intelligent reflecting surface enhanced wireless network via joint active and passive beamforming," *IEEE Transactions on Wireless Communications*, vol. 18, no. 11, pp. 5394–5409, 2019.
[40] D. Selimis, K. P. Peppas, G. C. Alexandropoulos, and F. I. Lazarakis, "On the performance analysis of RIS-empowered communications over Nakagami-m fading," *IEEE Communications Letters*, vol. 25, no. 7, pp. 2191–2195, 2021.

**Sajjad Nassirpour** received the B.Sc. degree in Electrical Engineering from Shiraz University, Shiraz, Iran, in 2011, and his M.Sc. degree in Electrical Engineering from Iran University of Science and Technology, Tehran, Iran, in 2014. He is currently pursuing the Ph.D. degree with the Department of Electrical Engineering at the University of Colorado, Denver. His research interests include network information theory, wireless communications, machine learning, and applications of coding theory in high-performance computer memory systems. He has received the Best Paper Award at the IEEE Computing and Communication Workshop and Conference (CCWC) in 2020.

**Alireza Vahid** (Senior Member, IEEE) received the B.Sc. degree in electrical engineering from Sharif University of Technology, Tehran, Iran, in 2009, and the M.Sc. and Ph.D. degrees in electrical and computer engineering from Cornell University, Ithaca, NY, in 2012 and 2015, respectively. From 2015 to 2017, he worked as a postdoctoral research scientist at the Information Initiative at Duke University, Durham, NC, and from 2017 to 2023, he was an assistant professor of Electrical Engineering at CU Denver. He is currently a Gleason Chair associate professor of Electrical and Microelectronic Engineering at Rochester Institute of Technology. His research interests include network information theory, wireless communications, and data storage. Dr. Vahid received the 2015 Outstanding PhD Thesis Research Award from Cornell University, the Qualcomm Innovation Fellowship in 2013, the Lab Venture Challenge Award in 2019, and SONY faculty innovation award in 2021. He currently serves as an associate editor for IEEE Communications Letters.

**Dinh-Thuan Do** (Senior Member, IEEE) received the B.S., M.Eng., and Ph.D. degrees in communications engineering from Viet Nam National University (VNU-HCMC), Vietnam, in 2003, 2007, and 2013, respectively. Before joining the University of Mount Union, he was with the University of Colorado Denver, Denver, Colorado, as a Postdoctoral Fellow in 2022. He also worked as a Research Scientist with The University of Texas at Austin, Austin, TX, USA, in 2021 and as an Assistant Professor with Asia University, Taichung, Taiwan, from 2020 to 2021. He published one textbook and five edited books. He has authored or co-authored over 100 technical papers published in peer-reviewed international journals (SCIE). His research interest includes signal processing in wireless communications network, reconfigurable intelligent surfaces, NOMA, UAV network, satellite system, physical-layer security, device-to-device transmission, and energy harvesting.

Dr. Thuan was a recipient of the Golden Globe Award from the Vietnam Ministry of Science and Technology in 2015 (Top 10 talented young scientists nationwide). He got the Creative Young Medal in 2015. He was named to the top list of 14 Highly Cited Scientists at Asia University in 2021. He was rewarded as the Best Editor of ICT Express in July 2023. He is serving as an Associate Editor in IEEE TRANSACTIONS ON VEHICULAR TECHNOLOGY and Computer Communications.

**Dinesh Bharadia** (Member, IEEE) received the bachelor's degree in electrical engineering from the Indian Institute of Technology, Kanpur, in 2010, and the M.S and Ph.D. degree from the Electrical Engineering Department, Stanford University, in 2013 and 2016, respectively. His Ph.D. thesis invalidated a long-held assumption in wireless communication by building full-duplex radios. From 2013 to 2015, he was a Principal Scientist with Kumu Networks, where he worked to commercialize his research on full-duplex radios, building a product that underwent successful field trials at Tier 1 network providers worldwide like Deutsche Telekom and SK Telecom. From 2016 to 2017, he was a Post-Doctoral Associate at MIT, after receiving his Ph.D. from Stanford University. From 2018 to 2022, he held an Assistant Professor position for four years at UC San Diego, and received early promotion to a Tenured Professorship. He is currently an Associate Professor at UC San Diego, the Director of the Wireless Communication Sensing and Networking Group (WCSNG), and part of several centers. At UC San Diego, his group WCSNG designs and prototypes systems for Wireless Communication, Computing, Sensing, Networking, and sensor design with applications to privacy, security, robotics, health, and everyday life. Much of the group's research has inspired new research areas for border communities: communication theory, circuits, RFIC, and robotics. Much of his research has been translated into startups and commercial products (Haila, Kumu Networks, Totemic Labs). In the last five years, the WCSNG research group has received multiple awards from NSF, industry funding, and DoD funds, allowing the group to train and sustain more than 40+ students at any time, training the next generation of talented engineers and scientists. In recognition of his research, he was named a Marconi Young Scholar for Outstanding Wireless Research and awarded the Michael Dukkakis Leadership Award. He was also named as one of the top 35 innovators under 35 globally by MIT Technology Review in 2016 and worldwide by Forbes 30 under and 30 for Science category in 2018. He received the Thomas and Sarah Kailath Stanford Graduate Fellowship and a Gold Medal at the IIT Kanpur for graduating at the top of his class.